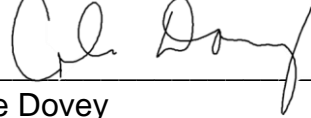


**Investigating Potential Regulators of TFIIIC-dependent Boundary Function in
*Schizosaccharomyces pombe***

Emma K Carlson
Molecular Biology
Dr. Jennifer Garcia

Primary Reader:  _____
Jennifer Garcia

Secondary Reader:  _____
Cole Dovey

Abstract

Gene expression, which is essential for cell function, can be controlled by packing of DNA into domains of accessible or inaccessible DNA. In eukaryotic cells, DNA is wrapped around histone proteins to form chromatin. Heterochromatin, is one type of chromatin that is packaged tightly and inaccessible for transcription. It is heavily modified to reduce accessibility of DNA to make large regions of chromatin transcriptionally silent. Modification of the 9th lysine of histone H3, repressive histone methylation, propagates along heterochromatin causing transcriptional silencing; unlimited spread of this repressive H3K9me will improperly silence neighboring regions of chromatin, thus interfering with gene expression. In eukaryotes like *Schizosaccharomyces pombe*, the spread of silencing can be prevented by specific DNA elements called boundary elements. Some boundary elements require the action of the RNA polymerase III transcription factor, TFIIC. However, other factors critical for TFIIC-dependent boundary element function remain unknown. Previously, our research employed a genetic screen and identified ten mutants that are potential regulators of this pathway. We confirmed by Sanger sequencing that four screen hits contained mutations in the following genes: *sda1*, *cog5*, SPNCRNA.189, and *vac7*. Also, to test that these mutants had impaired boundary function, we quantified levels of H3K9me over a reporter gene that monitored boundary activity in these four mutagenized strains. Preliminary ChIP assays on the original mutagenized strains showed three mutants, *sda1*, *cog5*, and *vac7*, had more repressive histone methylation over the boundary reporter gene than in the wild type reporter strain where the boundary elements was still functional. Also, to confirm that the effects we had observed in the original mutagenesis were due to the identified point mutations, we attempted to use the CRISPR/Cas9 system and homologous recombination to reintroduce the identified mutants into boundary function reporter strains. Though each cloning technique used will need optimization, we successfully deleted SPNCRNA.189 by homologous recombination. In the future, ChIP analysis on the boundary reporter strain re-introduced with candidate mutants will help identify factors that contribute to

boundary function and give insight to mechanisms by which boundary elements limit the spread of repressive histone methylation.

Introduction

Heterochromatin vs. euchromatin

Gene silencing plays a critical function for the genome by modulating gene expression to promote proper cell function. To understand this control, we must understand how the DNA is packaged to mediate interactions necessary for transcription. In eukaryotes, DNA is wrapped around histone proteins to compact and organize the DNA into structures called chromatin. Chromatin can be differentiated into two forms: euchromatin and heterochromatin. Euchromatin contains DNA that is highly transcribed, gene-rich and highly accessible. When the DNA is accessible like in euchromatin, the transcriptional machinery can readily access DNA sequences such as promoter elements and transcription factor binding sites, allowing for transcription to occur in euchromatin. Heterochromatin contains DNA that is transcriptionally silent, gene-poor and inaccessible. Conversely, access to DNA in heterochromatic regions prevent the transcription machinery from binding DNA elements, effectively silencing those regions of the genome [1].

In general, the regulation of DNA accessibility for heterochromatin is important particularly around centromeric regions, telomeres, and in genes required for specific cell-types or specific growth phases [1]. Heterochromatin is especially vital as it stabilizes repetitive DNA elements found in the genome to prevent undesired recombination can occur leading to increased genome instability [1]. Additionally, heterochromatic gene silencing reduces transposon movement in the genome as heterochromatic silencing prevents the expression of retrotransposons, which encoded gene products required for their movement. Additionally, cell development relies on heterochromatin to silence genes that are not utilized in differentiated

cells. Dysregulation of heterochromatin in the genome can lead to cellular dysfunction, disease, or even cell death.

To differentiate euchromatin from heterochromatin and allow for efficient regulation of DNA accessibility, the cell modifies the histone proteins with specific post-translational modifications [1]. Heterochromatin is marked by repressive histone methylation to the N-terminus of the histone H3 tail to mediate transcriptional silencing. Histone modifications, like repressive methylation, are read by proteins called reader proteins that recruit modifiers to impart DNA accessibility changes to mediate the specific transcriptional state dictated by the modification. The type of repressive histone methylation within heterochromatic domains can further define two distinct types of silent chromatin: facultative or constitutive heterochromatin. The facultative heterochromatin consists of protein-coding genes that were previously expressed but become silent as cells specialize. Constitutive heterochromatin, consists of regions of the genome which are never expressed in any cell-type. In *Schizosaccharomyces pombe*, constitutive heterochromatin consists of the pericentromeric region, sub-telomeric regions, and the silent mating type locus [1]. These regions of heterochromatin are preserved upon cell division and passed down epigenetically through establishment and maintenance of each repressive histone methylation mark.

Repressive histone methylation: Histone H3 Lysine9 methylation.

The two most prominent forms of repressive histone modifications associated with heterochromatin are H3K9 and H3K27 methylation. Though histone methylation can be found in euchromatin to mediate transcription, we will focus on forms of histone methylation found in heterochromatin. Generally, repressive histone methylation involves the covalent addition of one to three neutral methyl groups to a lysine residue of the N-terminal histone tail; where lysine can be methylated up to three times by histone lysine methyl transferases (HKMTs) [1]. The addition of the methyl group(s) does not change the charge of lysine side chain, but rather prevents histone acetylation (which destabilizes interactions between the histones to the DNA) from

occurring resulting in more compact histone DNA structure. Repressive histone methylation recruits reader proteins, which then bring chromatin modifiers such as histone deacetylases (HDACs; removes histone acetylation) and chromatin remodelers that promote chromatin structures that are less accessible.

Histone H3 Lysine9 methylation (H3K9me) is found in constitutive heterochromatin that results from the addition of 1-3 methyl groups to the 9th lysine of the H3 histone tail. Facultative heterochromatin is marked by methylation of histone H3 Lysine 27 residue. H3K9me is the most abundant histone modifications while H3K27me is not present in the single cell organism, *S. pombe* [1,2]. *S. pombe* relies on H3K9me to mediate transcriptional silencing over pericentromeric regions, telomeres, and the mating type (*mat*) locus [3,4]. Heterochromatin formation at these sites is mediated by an initial H3K9me event and is best understood for the pericentromeric regions and the *mat* locus. Just after cell division within these regions, inverted repeats in the pericentromeric regions or the cenH region in the *mat* locus, are transcribed causing the recruitment of RNAi machinery to these transcripts [5]. Small interfering RNAs are made from the resulting transcripts and instigate heterochromatin formation [3,5,6]. Through a series of events the H3K9 histone methyltransferase is recruited to the site of transcription. H3K9me is then placed, resulting in the recruitment of a reader protein, Swi6. This event then recruits the H3K9 histone methyltransferase to methylate neighboring histones and initiates the spread of H3K9me in a sequence-independent manner, continuing laterally along the chromatin until inhibited [4].

Methylation spread in H3K9me is driven by this binding of the Swi6 protein, which belongs to the HP1 family in mammals [2]. HP1 proteins, like Swi6, are known to interact with histone methyltransferases. Also, Swi6 binds to the H3K9me tail and recruits deacetylases, which remove histone acetylation within heterochromatin for H3K9me to propagate along the genome [2,3]. Although H3K9me spread is essential to silence heterochromatin, if not contained

to those regions neighboring euchromatic domains can be silenced. This uncontained spread can interfere with proper gene expression [4].

Another element involved in the spread of H3K9me is the Clr4 histone methyltransferase in *S. pombe* that writes the H3K9me mark on histones by directly associating with its reader protein, Swi6 [2]. Clr4 is a part of the methyltransferase complex, called ClrC [5]. Formation of the *mat* locus heterochromatic domain can also be initiated in an RNAi-independent manner where DNA binding proteins recruit ClrC to silence DNA elements within the *mat* locus. Additionally, in *S. pombe*, ClrC can artificially tether to euchromatic domains of the genome and can initiate heterochromatin nucleation and spread [2], suggesting that once heterochromatin formation is initiated by the recruitment of ClrC, it can spread over any region of the genome to induce transcriptional silencing.

To prevent improper nucleation and spread from heterochromatic DNA domains, strategically located DNA sequences called boundary elements demarcate euchromatin-heterochromatin boundaries. In *S. pombe*, boundary elements are sequences found namely at the borders of the pericentromeric regions, telomeres, and the *mat* locus where they are required for limiting H3K9me spread [4]. These boundary elements are also defined as insulators of heterochromatin. In *S. pombe*, these sequences require the activity of Epe1 and TFIIIC in their respective pathways to prevent spread.

Epe1 and TFIIIC pathways for insulating the genome from the spread of repressive methylation.

Epe1 and TFIIIC function to limit H3K9me spread, but their mechanisms of action are still not fully understood [4]. Epe1 is part of the JmjC protein family that disrupt heterochromatin by catalyzing histone demethylation, however, Epe1 does not exhibit *in vitro* demethylase activity [5]. Epe1 function is mediated by binding specifically to Swi6, which is critical for H3K9me propagation along the genome [2,4] and recruits chromatin remodelers to acetylate histones [7]. Epe1 is enriched at boundary elements preventing H3K9 methylation spread but also has been found in heterochromatic regions. To prevent global euchromatinization by Epe1,

the E3 ubiquitin ligase Cul4-Rik1^{Dos1/Dos2}, ubiquitinates and targets Epe1 found in heterochromatin for degradation by the proteasome, effectively removing Epe1 from heterochromatin [6]. Overall, the mechanism of how the Epe1 pathway acts to limit repressive histone methylation within euchromatic domains is generally well defined.

The second pathway that limits H3K9me spread from heterochromatin in *S. pombe* is mediated by the RNA polymerase III transcription factor TFIIC. TFIIC interacts directly with several boundary elements in the genome, including the ones surrounding the pericentromeric region, sub-telomeric regions, and silent mating type (*mat*) locus [4]. Also, TFIIC is known to bind DNA elements that localize at nuclear periphery, suggesting a possible mechanism to mediate boundary function by tethering heterochromatic domains against a physical barrier such as the nuclear periphery to prevent H3K9me spread [8]. The *mat* locus, the region of our focus in this study, is flanked by two inverted identical repeats called *IR-R* and *IR-L*. Each *IR* element contains several DNA elements called the B-box elements which are bound by TFIIC (Figure 1), allowing for heterochromatin insulation at the mating type locus [8]. Similarly, multiple tRNA genes can act as boundary elements around the *mat* locus in *S. cerevisiae* and the pericentromeric regions in *S. pombe* as they contain B-box elements bound by TFIIC. Overall this indicates that the B-box elements bound by TFIIC play an important role in boundary function. For tRNA sequences that act as boundary elements, they are known to recruit TFIIC and are typically transcribed by RNAPIII which initiate recruitment of histone acetylases and chromatin remodelers [9]. TFIIC is critical in mediating RNAPIII transcription of tRNAs in boundary elements, however, whether or not RNAPIII is required for the establishment of a functioning boundary element is not known as RNAPIII binding is not required for boundary function at *IR* elements [8]. Though other elements are necessary for TFIIC function, these factors seem to be either only periodically present or virtually unknown, such as RNAPIII. Interestingly, the boundaries that utilize TFIIC containing B-boxes for the purpose of boundary function are conserved, including at the *IR* elements, indicates that the TFIIC pathway is an

important stabilizer and regulator of the genome [5]. Though TFIIIC is confirmed to be an important gene regulating pathway, factors required for RNAPIII-independent boundary function, or TFIIIC-dependent *IR* boundary function, need to be discovered to further our understanding to limit H3K9 methylation spread.

Both of the Epe1- and TFIIIC-dependent pathways actively prevent H3K9me spread, and recent studies have determined that these two pathways are redundant and act in parallel to each other [4]. For example, Garcia *et al.* determined that the deletion of both the Epe1 protein and the B-box elements in the *IR* element was necessary to completely deactivate the *IR* boundary element function; while deletions of one or the other retained limited boundary function [4]. More significantly Garcia *et al.* demonstrated that the complete removal of boundary function at just one boundary element (*i.e.* a single *IR* element), led to a toxic spread of H3K9me silencing into neighboring euchromatic regions. Collectively, the existence of two parallel and redundant pathways and the impact of deactivating one boundary element stresses the significance of regulating in heterochromatic spread. Mapping out the complete mechanism of each pathway will be crucial to understanding gene silencing in *S. pombe* and conserved mechanisms of genetic regulation and homeostasis. Bao *et al.* has already done some research on narrowing down factors involved in the Epe1 pathway so our research focusses on the much less studied mechanisms of the TFIIIC pathway [7].

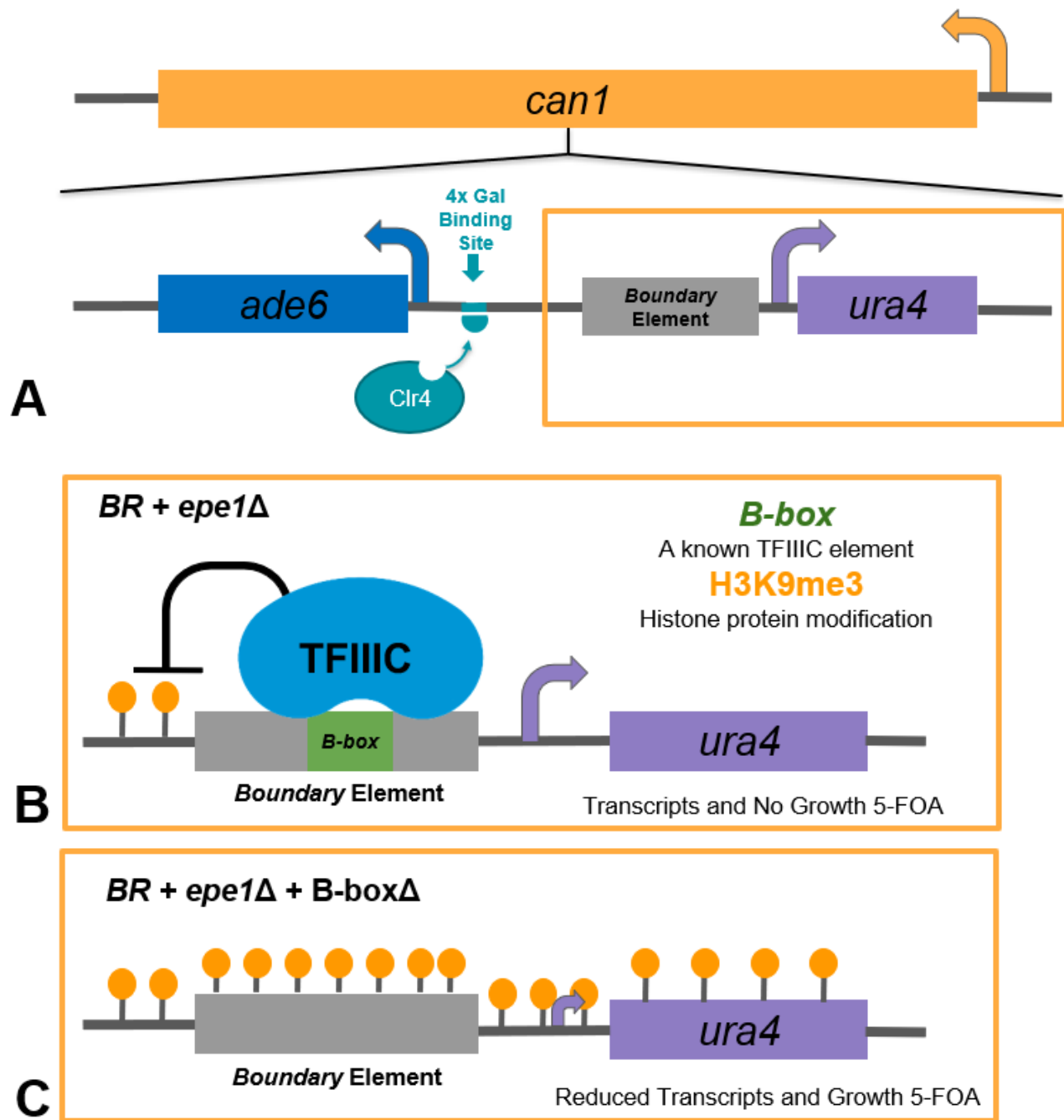


Figure 1: Model of the Full TFIIC boundary reporter and the General Mechanism with and without the *B-boxΔ*. (A) The full TFIIC boundary reporter construct within the *CAN1* locus containing *ADE6* for reporting H3K9me spread, *URA4* for reporting boundary function, the boundary element, and a Gal binding site so Clr4+Gal binding domain will localize and initiate

H3K9me. (B) The TFIIIC boundary reporter (BR) eliminates parallel *epe1* pathway function. An active boundary element halts heterochromatin spread *URA4* is expressed and incapable of growing on 5-FOA media. (C) An inactive boundary element (caused by the deletion of the B-box) allows H3K9me spread and *URA4* becomes silenced.

Identifying factors in the TFIIIC-dependent Boundary Pathway.

To further gain mechanistic insight into TFIIIC-dependent boundary function, we focused efforts identifying other factors necessary for *IR* boundary function by performing a genetic screen. A strain was created to phenotypically observe *IR* boundary function solely dependent on TFIIIC-mediated boundary function. To allow for phenotypic observation of TFIIIC boundary function, reporter genes were designed and inserted into the *CAN1* locus as it is a gene that has a selectable phenotype when disrupted (*i.e.* growth on PMG + Canavanine plates) and no essential genes were in close proximity to *CAN1*. *URA4* was used to report on boundary function while *ADE6* reported H3K9me silencing activity. Downstream of *URA4* and upstream of *ADE6*, the DNA sequence of the boundary element to test (*i.e.* *IR* element) was inserted [4]. Then between the boundary element and *ADE6*, 4- Gal4 UAS sequences were inserted to tether Clr4 fused to a Gal DNA binding domain (Figure 1A). This tethered Clr4 induced H3K9me at this site and its spread. When grown on nutrient rich media contain 5-FOA, the gene product of *URA4* metabolizes 5-FOA into a toxic compound that results in cell death. The opposite is true when the *URA4* is silenced. Garcia *et al.* demonstrated that this strain was able to mimic *IR* boundary function at the *CAN1* locus. To observe TFIIIC-dependent boundary function, the reporter strain above harbored a deletion of *Epe1* (*epe1* Δ ; Figure. 1B). When the boundary element is actively working with TFIIIC mechanisms to halt heterochromatin spread, *URA4* is expressed and this *epe1* Δ boundary reporter strain is incapable of growing on 5-FOA media. When boundary element function is disrupted, *URA4* becomes silenced as H3K9me spread

over the boundary element [10]. By mutagenizing the *epe1*Δ boundary reporter strain using ethyl methane sulfonate (EMS), we can screen for DNA mutants that affect *IR* boundary function. This mutagenesis screen yielded ten potential hits that exhibited disrupted TFIIIC boundary function. The genomic DNA from the ten hits were sequenced to identify EMS-induced mutations. Whether these mutants represented true factors involved in TFIIIC-dependent boundary function remained unclear as they may represent false positives. I aimed to validate whether or not these EMS-induced mutants represented mutations in factors necessary for TFIIIC-dependent boundary function or false positives.

Of the 10 mutants with identified mutations, 6 mutants were eliminated from analysis as 4 were false positives that affect 5-FOA metabolism and 2 did not contain the identified point mutation. I attempted to create constructs of the 4 potential mutants, *sda1-G1160T*, *cog5-G23T*, *SPNCRNA.189-G1004A*, and *vac7-A381G*, to reintroduce the mutations we identified into the original reporter strain by CRISPR or homologous recombination of the point-mutations or gene deletions. Additionally, I optimized Chromatin Immunoprecipitation (ChIP) to quantify levels of H3K9me as we expect to see repressive methylation spread over the *ura4* reporter gene. We found that mutants in *sda1*, *cog5*, and *vac7* showed more H3K9 methylation over *ura4* than the wild-type boundary reporter harboring full TFIIIC boundary function. After further analysis of these four mutations and increasing the precision of the assays, we will be able to determine how they affect the TFIIIC pathway, and, thus, their importance to gene regulation in our model organism.

Materials and Methods.

Pinning Assay.

Cultures were started in YS media and grown at 30°C on a rotor drum overnight. The cultures were back diluted to an OD₆₀₀ of 0.4 in 300μL in a 96-well plate. Five 1:6 serial dilutions of OD₆₀₀ of 0.4 were made with warmed YS media. The pinner was sterilized with ethanol and

open flame. After cooling the tool, the dilutions were stamped onto a warmed YS plate. It was then incubated at 30°C overnight and the results were photographed using an iPhone.

PCR amplification of target genes.

A PCR reaction containing 1X Phusion HF buffer, 0.2mM dNTPs, 0.5µM gene specific primers (Table 2. – Target Gene Amplification) and 0.02U/µL Phusion DNA polymerase. 500 -1500ng DNA of yeast genomic DNA, prepared using a yeast DNA extraction protocol, was used in each PCR. Reactions were denatured at 98°C for 30 seconds and were run for 25 cycles (98°C for 10 seconds and 48-52°C for 30 seconds, 72°C for 17 or 30 seconds) ending with a final extension at 72°C for 8 minutes. The product was checked via gel electrophoresis in a 1% agarose gel at 120V for 40 minutes.

Sanger Sequencing.

All of the mutants were sent to a sequencing center in reactions containing 50ng of yeast DNA surrounding the point mutations purified through yeast DNA extraction, or 800ng of plasmid, and 5µM sequencing primers (Table 2. - Sequencing).

Yeast DNA Extraction.

Yeast cells were grown either in liquid or plate cultures. The liquid cultures were spun down at 3000rcf, the supernatant was discarded, and 200µL Breaking Buffer was added to either the pellet or a single colony along with an equivalent amount of zirconia beads and equilibrated phenol. The mix was vortexed for 3 minutes and centrifuged for 1 minute at the maximum speed. 200µL of water was added and spun for 10 minutes at 3000rcf. DNA preps that were to be used for transformation via electroporation, the aqueous phase was transferred to 500µL chloroform, vortexed for 3 minutes, and 200µL of water was added. The aqueous phase was transferred into 1mL of ethanol. Preps were then spun down again for 5 minutes at 3000rcf and the supernatant was removed again. The pellet was washed with 500µL 70% ethanol and spun for 5 minutes at 3000rcf. The pellet was air dried, with a kimwipe covering the microcentrifuge tube, and resuspended in 50-100µL water.

Guide RNA site insertion into the pMZ377 plasmid.

Reactions contained 2% DMSO, 1x Phusion HF buffer, 0.2mM dNTPs, 0.4 μ M primers (Table 2. – gRNA insert into pMZ377), 5ng pMZ377, and 0.02U/ μ L Phusion polymerase, except the *vac7* sgRNA reaction which was set up without DMSO and replacing Phusion HF buffer for GC buffer. Reactions were run through a thermocycler at an initial denaturation of 98°C for 2 minutes and 25 cycles (98°C for 10 seconds, 55 or 60°C for 30 seconds, 72°C for 5.5 minutes), ending at 72°C for 5 minutes. The product was checked via gel electrophoresis in a 1% agarose gel at 120V for 40 minutes. The constructs were then transformed into *E. coli* using the NEB high efficiency protocol [11].

Single guide RNA site scramble in mutant strains.

PCR reactions containing 1x Phusion HF buffer, 0.2mM dNTPs, 0.4 μ M primers (Table 2. – sgRNA Site Scramble), 250ng yeast genomic DNA, and 0.02U/ μ L Phusion polymerase were run in a thermocycler at 98°C for 30 seconds, cycled 25 times (98°C for 10 seconds, 50°C for 30 seconds, 72°C for 30 seconds), and completed at 72°C for 8 minutes. PCR products were checked via gel electrophoresis in a 1% agarose gel at 120V for 40 minutes. The two segments were combined in a 1:1 molar ratio with the average amount of DNA being 50ng. 1x Phusion HF buffer, 0.2mM dNTPs, 0.5 μ M primers (Table 2. – Confirm sgRNA Scramble), and 0.02U/ μ L Phusion DNA polymerase. All reactions were run in a thermocycler at 94°C for 2 minutes, cycled 30 times (94°C for 20 seconds, 52°C for 20 seconds, 72°C for 40 seconds), and finished at 72°C for 10 minutes. The product was checked via gel electrophoresis in a 1% agarose gel at 120V for 40 minutes. The products were then gel purified and amplified again under identical conditions to increase yield of a single product.

PCR amplification of pAG32 with target gene homology regions.

PCR reactions included 1X Phusion HF buffer, 160 μ M dNTPs, 0.2 μ M of each primer (Table 2. – hphMX Deletion Set1), 2ng/ μ L of plasmid DNA, and 0.01U/ μ L Phusion DNA polymerase. The thermocycler was run at 98°C for 30 seconds, cycled 30 times (98°C for 10 seconds, 42-58°C

for 20 seconds, 72°C for 45 seconds), and completed at 72°C for 8 minutes. The product was checked via gel electrophoresis in a 1% agarose gel at 120V for 40 minutes. The PCR was duplicated exactly with the DNA product of the first reaction and the second set of primers. (Table 2. – hphMX Deletion Set2).

Restriction Digest.

0.5-1µg of plasmid DNA with 20U/µL of selected restriction enzyme (Table 3) was added in 1X NEB Cutsmart Buffer [12]. The reaction was gently mixed and incubate for at least 90 minutes at 37°C. Results were visualized using gel electrophoresis.

Fusion PCR.

PCR products for each individual segment were added in a 1:1 molar ratio up to 2ng/µL in 1X GC Phusion buffer, 0.2mM dNTPs, 50mM each primer (Table 2. – Full Fusion), and DNA Phusion polymerase. Reactions were run in the thermal cycler at 94°C for 2 minutes, cycled 30 times (94°C for 20 seconds, 52°C for 20 seconds, 72°C for 2 minutes), and at 72°C for 10 minutes. The product was checked via gel electrophoresis in a 1% agarose gel at 120V for 40 minutes.

Sequence and ligation independent cloning, SLIC, protocol.

SmaI-digested pRS416 (vector) and overlapping PCR product (insert) were combined in a molar ratio 1:2 in 1x 2.1 NEB Buffer, >0.5µL T4 DNA polymerase, and incubated at room temperature for 10-45 minutes, followed by a 10-minute incubation on ice. NEB high efficiency *E. coli* cells were thawed and 5µL of the ligation reaction was added to the cells and incubated on ice for 20 minutes. Transformations were then heat shocked for 30 seconds at 42°C and cooled on ice for 5 minutes. 950µL of warm SOC was added the cells and incubated at 37°C for 1 hour. The mixture was then centrifuged at 3000xg for 1 minute and 800µL of supernatant was removed. Cells were resuspended in remaining supernatant, spread on warmed LB plates with ampicillin, and incubated at 37°C overnight [11,12].

High Efficiency NEB Transformation.

NEB 5-alpha Competent *E. coli* cells were thawed for 10 minutes. About 100ng of plasmid DNA was carefully mixed into the cells and incubated on ice for 30 minutes. Cells were heat shocked for 30 seconds at 42°C followed by a five-minute incubation on ice. 950µL of SOC was added then placed in a 37°C incubator while nutating or shaking for 1 hour. 50-100µL was plated on selection plates, LB with 1X carbomycin, and left overnight at 37°C [11].

Bacterial Electroporation Transformation.

A liquid culture of *E. coli* was grown for 16 hours at 37°C while shaking then approximately 1000µL was plated on an LB plate and grown for an additional 4-6 hours at 37°C. *E. coli* was collected from plate by washing cells from plate using 1ml of sterile water and the tube was centrifuged at 5000xg for 5 minutes at 4°C three times. After the final centrifugation, the pellet was suspended in water remaining from pouring out the last 1mL wash, 1µg of plasmid DNA, and transferred to a chilled 0.2cm gap cuvette. The Bio-Rad Gene Pulser II with Pulse Controller Plus was set to 1.8kV, 25µF, time constant = 5ms, was used to electroporate the cells. Immediately after electroporation, 1mL LB broth was added and cells were grown for 30 minutes while rotating at 37°C. Cells were plated on EMM-Leu or PMG-Leu overnight at 37°C [13].

S. pombe transformation protocol with PEG/LiOAc.

S. pombe grown in YS media with glucose overnight at 30°C were back diluted to an OD₆₀₀ of 0.2. Once in the late log phase, OD₆₀₀ 0.6-1.0, the cells are collected via centrifugation at 2000rpm for 5 minutes, washed in 1mL water and then 1 mL LiTE (0.1M LiOAc, 1xTE at pH 8) before a final suspension in 100µL of the LiTE solution per transformation. 2µg of DNA is added with a 0.1mg/mL carrier DNA to cells and allowed to sit for 15 minutes. 500µL of PEG/LiOAc (40% PEG 3350, 100mM LiOAc, 1x TE) was added and the transformation was placed in 30°C for 50 minutes. 50µL of DMSO was added before the mixture was heat shocked for 10 minutes at 42°C and spun at 2000rpm for 3 minutes. The resulting pellet was resuspended in YS and plated on EMM-Leu for a two-day incubation at 30°C.

S. pombe transformation protocol using PEG3350.

S. pombe grown in YS media with glucose overnight at 30°C was diluted 1:20 in fresh media and grown for additional 3-5 hours before being spun down at 3000rcf for 5 minutes. 250µL 50% PEG3350 resuspended the pellet. 3.3µg/mL carrier DNA was added with 0.12M LiOAc and 6.7µg/mL DNA, and the reaction was heat shocked at 42°C for 20 minutes. After the cells were spun down at 3000rcf for 30 second the pellet was resuspended in YS media, plated onto selective media, and grown for 3 days at 30°C.

S. pombe transformation protocol with nitrogen starved cells.

S. pombe grown at 32 °C in EMM overnight was back diluted to an OD₆₀₀ of 0.1 and grown to an OD₆₀₀ of 0.6. Cells were pelleted at 1800xg for 3 minutes and washed twice in EMM-N. Cells were resuspended in 50mL of EMM-N and then incubated for 2 hours at 25°C. Ice was used to cool the culture for 15 minutes and cells were kept at 4°C for the rest of the transformation. Cells were spun at 1600xg for 5 minutes and washed three times with water. 0.5 mL ice-cold solution (30% glycerol, 0.1M LiOAc (pH 4.9)) was used to resuspend the cells. 12.5µL aliquots were placed on ice for 2 minutes before storage at -80°C. The samples were prepared for transformation by heating at 40 °C for 2 minutes and adding 125µg/mL carrier DNA, 12.5µg/mL plasmid DNA, and 145µL 50% PEG4000. The mixture was incubated for 15 minutes at 42°C, spun for 3 minutes at 1600xg. The pellet was suspended in 1mL EMM-N and incubated for 16 hours without shaking. The pellet was collected using the same centrifugation conditions and plated on EMM-Leu with a 4-day incubation at 32°C. The smallest colonies were re-streaked on YES plates.

S. pombe transformation protocol using modified LiOAc.

S. pombe grown in YS media to an OD₆₀₀ of 0.5 was pelleted at 3000rpm for 3 minutes. 5mL of cells were used the first time and optimized to 50mL. The pellet was suspended in water, centrifuged for one second at maximum speed, washed and resuspended in 500µL LiTE (0.1M LiOAc, 1xTE). Then the reaction was set up as in the original LiOAc protocol. 260µL of PLATE

(40% PEG3350, 0.1M LiOAc, 1x TE) was mixed in and incubated for an hour at 30°C. 43µL DMSO was added, then the transformation was heat shocked at 42°C for five minutes, pelleted, and washed with water. The cell pellet was resuspended in water and plated on selection plates. Plates were grown for several days at 30°C (From Hyun Soo Kim, Keogh lab, AECOM).

S. cerevisiae high efficiency transformation for DNA ligation.

S. cerevisiae was grown in YPAD at 30°C overnight then back diluted to an OD₆₀₀ of 0.3 then grown for 3-5 hours at 30°C. The cells were pelleted at 3000rcf for 5 minutes then pellet was resuspended in 250µL 50% PEG3350. 3.3µg/mL carrier DNA was added with 0.12M LiOAc and 6.7µg/mL DNA. The transformation mix was heat shocked at 42°C for 20 minutes, spun at 3000rcf for 30 seconds, then the cell pellet was resuspended in YS. EMM-Leu selection plates were used to grow the transformants at 30°C for 1-2 days. After a yeast DNA extraction, the DNA was transformed into *E. coli* via the bacterial electroporation transformation of mass plasmid replication.

Cloning protocol used to create sda1/pRS416 construct.

pRS416 was placed in a restriction digest reaction with XbaI and PstI cutting at the insertion site and incubated overnight at 37°C. The reaction was heat inactivated 80°C for 20 minutes and purified with the Monarch® DNA purification kit. The insert, from the full fusion of sda1, and plasmid were combined in a 3:1 mass ratio in 1X T4 DNA ligase Buffer, 400U T4 DNA ligase were added to a 20µL reaction and incubated overnight at 16°C, or for 10 minutes at room temperature. The ligation was heat inactivated at 65°C for 10 minutes and chilled on ice. 1-5µL of the reaction was used for the high efficiency NEB transformation into competent cells. The transformation was plated on LB with carbomycin plates overnight at 37°C.

Bacteria Colony PCR.

An *E. coli* colony taken directly from the plate was placed in a PCR reaction. 1x Taq Reaction buffer, 200µM dNTPs, 0.2µM each primer (Table 2. – Insert Check), and 0.025U/µL PCR Taq DNA polymerase. In a thermocycler, the reactions were run at 95°C for 30 seconds, 30 cycles

(95°C for 30 seconds, 45-68°C for 1 minute, 68°C for 1 minute), and completing at 68°C for 5 minutes. The product was checked via gel electrophoresis in a 1% agarose gel at 120V for 40 minutes.

Chromatin Immunoprecipitation analysis of H3K9me with MNase Digest.

Cells were grown to an OD₆₀₀ between 0.75-0.85 at 30°C. Formaldehyde was added to a final 1% concentration and incubated, while shaking, for 20 minutes at growth temperature. 125mM glycine was then added and incubated for 5 minutes at room temperature. Cells were pelleted at 3000xg for 5 minutes at 4°C and washed with ice cold water. The pellet was resuspended in ice cold water and spun down at 3000xg, 4°C for 2 minutes. Finally, the pellet was flash frozen with liquid nitrogen and stored at -80°C.

The cells were spheroplasted by adding 1000µL BME mix (10µM BME in CES [50mM Citric acid/50mM NaHPO at pH 5.6, 40mM EDTA pH 8.0, 1.2M sorbitol]), 1000µL Zymo mix (5mg/mL zymolase in CES), and incubating at 30°C for 1 hour while rotating. Cells were spun down at 3000xg for 3 minutes at 4°C. Cells were washed twice with 2mL 1.2M sorbitol and recovered by centrifugation at 3000xg, 3 minutes at 4°C.

Next pNP-S buffer (1.2M sorbitol, 10mM CaCl₂, 100mM NaCl, 1mM EDTA pH 8.0, 14mM beta-mercaptoethanol, 50mM Tris pH 8.0, 0.075% NP-40, 5mM spermidine, 0.0038% Sigma fungal protease inhibitors mix) was added to bring the spheroplasts to a final volume of 1mL and divided into 2 500µL aliquots and one small aliquot, approximately 50µL. The larger aliquots were mixed with 250µL pNP-S buffer and 75U/µL units of MNase (Worthington). This mixture was incubated at 37°C for 15 minutes and quenched with 1/10 volume of 0.5M EDTA, pH 8.0, on ice.

MNase digest aliquots, at 4°C, had 250µL cold 4x Buffer L (200mM HEPES-KOH at pH 7.5 [200mM Tris-Cl and 1.5M NaCl in TBS], 560mM NaCl, 4mM EDTA, pH 8.0; 4% Triton X-100, 0.4% NaDOC) added. 800µL of the sample were set aside for the immunoprecipitation (IP) and the rest was used as the whole cell extract (WCE), saved at -20°C. The IPs were pelleted at

maximum speed for five minutes. Supernatant was moved to a new tube and primary antibody (2 µg of anti-(H3K9 di-Me) Ab1220), was added. The mixture was nutated overnight at 4°C. Per IP, a 150µL slurry of SureBeads magnetic beads were prepared by washing twice with 1mL 1X TBS, three times with 1mL ChIP lysis buffer (50mM HEPES-KOH pH 7.5, 140mM NaCl, 1mM EDTA, 1% Triton X-100, 0.1% NaDOC) with protease inhibitors (3.8µL/mL), and placed on ice for 5 minutes on a nutator between all washes. Beads were then resuspended in 100µL ChIP lysis buffer with protease inhibitors. 100µL of the prepared SureBeads magnetic beads was added to each IP and incubated at 4°C on a nutator. After 90 minutes, the supernatant was removed, and beads were washed. First 1mL of lysis buffer was added, the beads were nutated for 5 minutes at room temperature, and beads were separated from the lysis buffer using a magnetic tube rack. Lysis buffer was replaced with high salt lysis buffer (50mM HEPES-KOH pH 7.5, 500mM NaCl, 1mM EDTA, 1% Triton X-100, 0.1% NaDOC), beads were rotated for 5 minutes at room temperature, and separated from the high salt lysis buffer using a magnetic tube rack. This process was iterated with wash buffer (10mM Tris-Cl pH 8.0, 0.25M LiCl, 0.5% NP-40, 0.5% NaDOC, 1mM EDTA) followed by 1x TE. The beads were then suspended in 100µL elution buffer (50mM Tris-Cl at pH 8.0, 10mM EDTA at pH 8.0, 1% SDS) and incubated for 15 minutes at 65°C. The beads were centrifuged at maximum speed for 15 minutes at room temperature and supernate was transferred to a new tube. Beads were added to 150µL TE+0.67%SDS, centrifuged at maximum speed for 5 minutes, and combined with the first supernatant. 0.012U/mL Proteinase K was added and incubated at 65°C overnight.

Chromatin Immunoprecipitation analysis of H3K9me with Sonication.

The cell pellet was prepared the same as for the MNase protocol. After the flash freeze step, cell lysis was thawed and kept at 4°C. 500µL of ChIP lysis buffer with protease inhibitors and approximately 450µL of 0.5mm Zir/cilica beads were added. The VWR Bead Mill Homogenizer was used to bead break the cells. 6 rounds, each 30 seconds, were run with 2-minute pauses

between each round. A 23G1 needle was then used to puncture a hole in the base of the tube. This tube was further placed into one larger 5mL tube and centrifuged at 1000rpm for 3 minutes. The lysate was transferred and spun again at 8000rpm for 10 minutes. The pellet was saved and suspended in 300 μ L of Lysis buffer. The samples were then run through a Fisher scientific Sonic Dismembrator model 100 at a setting of 3 for 10 seconds with 2-minute rest on ice. Samples were centrifuged at 14000rpm for 10 minutes. Supernatant was saved and stored at -80°C. The supernate was thawed on ice and 500 μ L lysis buffer was added for each immunoprecipitate (IP) and whole cell extract (WCE). This was then separated into 500 μ L aliquots for observation. Antibody was added to the IPs. IPs, IP was performed and DNA recovery was done as described in the ChIP protocol using MNase Digest expect for the following changes: 30 μ L slurry of Protein A Dynabeads per IP were nutated for 2 hours, the first three washes were repeated, and beads were incubated at 70°C for 20 minutes after addition of elution buffer. Additionally, before the overnight incubation with Proteinase K, one tenth the volume of 10% SDS was added to the WCEs and spun at maximum speed for 5 minutes at 14000rpm. WCE supernatant was added to 0.012U/mL Proteinase K.

All prepared aliquots were purified with the Monarch® DNA purification kit, but water with 0.1 μ g/ μ L RnaseA was used instead of elution buffer. The purified DNA was incubated for an hour at 37°C.

RT-qPCR analysis of ChIP.

1X iTaq Supermix, 0.3 μ M forward and reverse primer (Table 2), and 3 μ L of ChIP DNA was analyzed using the Bio-rad CFX-96 Connect Real-time PCR System. The reaction was denatured at 95°C for 3 minutes, cycled 39 times (95°C for 20 seconds, 56°C for 20 seconds, 72°C for 40 seconds), and finished with melt peak conditions at 65°C for 5 seconds and 95°C for 20 seconds.

Results

Confirmed presence of four mutations suspected of inhibiting boundary function.

Previously, a genetic screen in *S. pombe* identified 10 potential hits that harbored mutations that possibly resulted in a loss of boundary function mediated by TFIIIC. Genomic DNA from these 10 hits were subjected to next generation sequencing and compared to the original strain to identify point mutations, insertions, or deletions within the genomic DNA that may be impairing boundary function. Four of the ten hits were eliminated immediately, as they were either silent mutations or mutations in the *ura4* biosynthesis pathway. Any mutations in the uracil biosynthesis pathway would affect the reporter that was used for genetic selection but not boundary function pathway, and therefore can be considered false positives.

After this initial analysis, the remaining genes with potential mutations included *sda1*, SPNCRNA.189, *cog5*, *sbg1*/SPNCRNA.1443, *kap104*, and *vac7*. To confirm if these strains with the identified mutations exhibited phenotypes of defective boundary function, we tested the growth of strains harboring those mutants on 5-FOA pinning assay. In our boundary reporter, the functional TFIIIC-dependent boundary element prevents the spread of H3K9me over *URA4*; the resulting Ura4 enzyme creates a toxic byproduct with 5-FOA and inhibits growth of *URA4* expressing cells. Conversely, if the boundary pathway is disrupted by mutations, methylation spreads over *URA4* and the cells will be able to grow in the presence of 5-FOA. Using a pinning assay (cell concentration decreases, from left to right), we compared the growth of the six potential screen hits and two controls, the *IR* boundary reporter + *epe1Δ* as a positive control and the *IR* boundary reporter + *epe1Δ* strain without B-boxes in the boundary element (*IR* boundary reporter + *epe1Δ* + *B-boxΔ*) as the negative control, on YS media with and without 5-FOA (Figure 2). YS is a growth media that will allow the proliferation of *S. pombe*, with or without boundary reporter function. Our positive control showed inhibited cell growth and the negative control had a renewal of cell growth on 5-FOA. We confirmed that six hits grew on

YS+5-FOA like the negative control, suggesting deactivation of the boundary element and methylation driven silencing of the *URA4* gene.

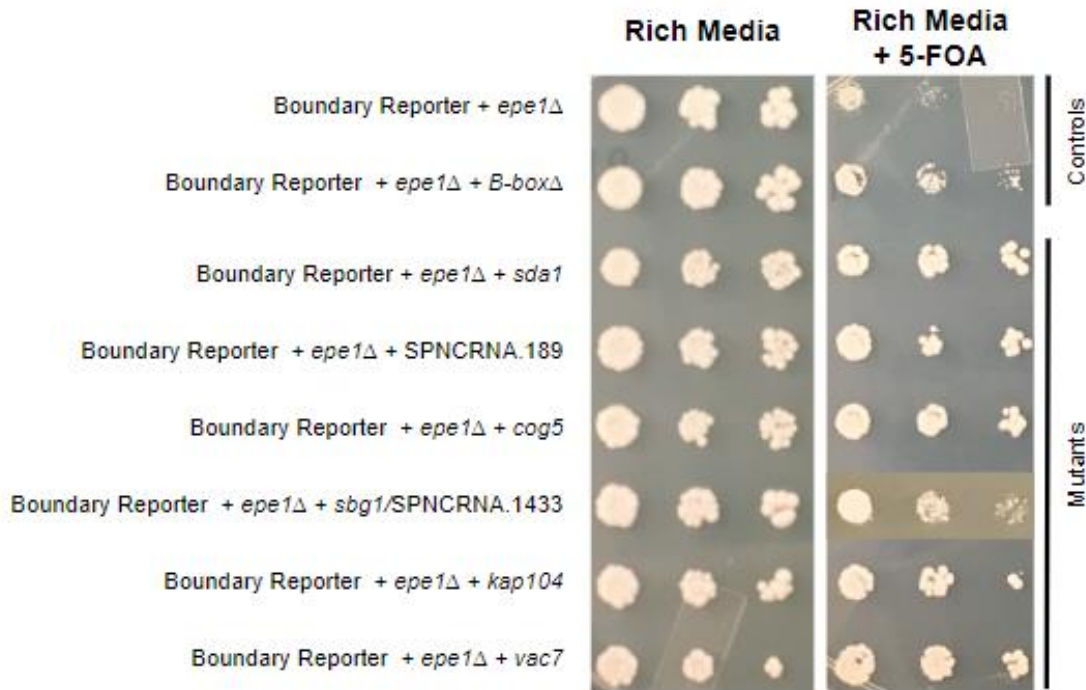


Figure 2: Pinning assay on rich media confirms methylation across *ura4* in mutant strains. Strains harboring suspected mutants were pinned onto rich media (YS) and YS + 5-FOA. Expression of the *URA4* in control strains on + 5-FOA creates a toxic byproduct that inhibits cell growth. Loss of *URA4* expression in mutants is indicated by growth on + 5-FOA.

To confirm the next generation sequencing results of each hit were truly present in each phenotypically observed hit, we prepared genomic DNA from each mutagenized strain. Sanger Sequencing was then performed on a single PCR amplified portion of the target gene around the suspected point mutations from the yeast genomic DNA (Figure 3A). This experiment confirmed the presence of the suspected point mutations in four of the six genes: *sda1*, SPNCRNA.189, *cog5*, and *vac7* via sequencing (Figure 3B). For the mutations we could not confirm, sequencing of *kap104* appeared to have two overlapping reads at first and was sent to

be re-sequenced. *kap104* was eliminated from further analysis because the point mutation did not appear in the second set of sequencing results. Also, the *sbg1* point mutation was not present in the sequencing results.

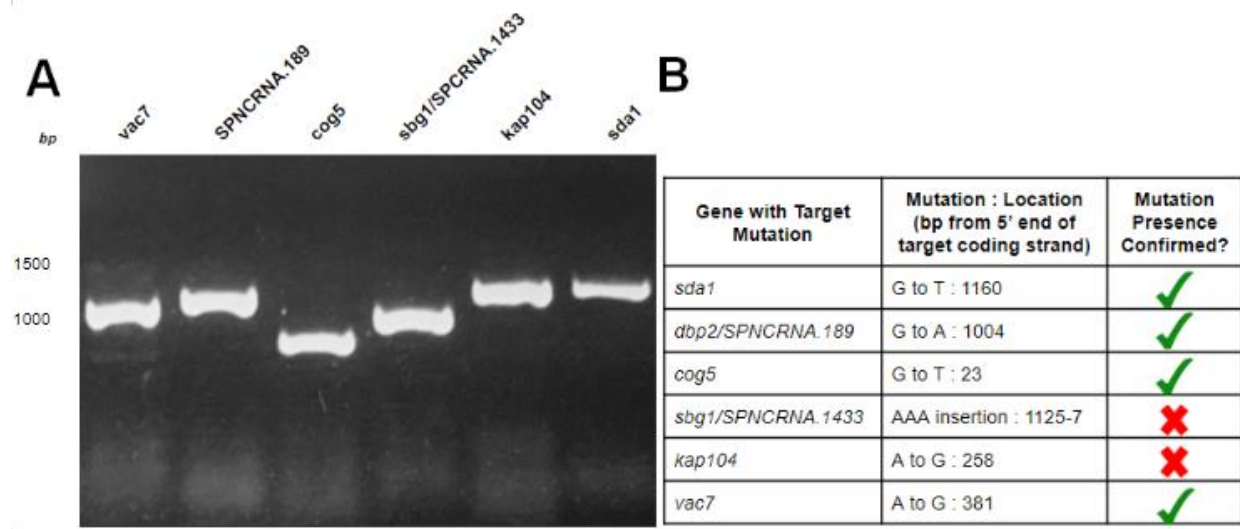


Figure 3: PCR amplification of mutant genes verifies size and confirming point mutations by sequencing. (A) PCR products amplified from genomic DNA isolated from EMS generated mutagenized *S. pombe* strains, and were run on a 1% agarose gel. (B) Suspected point mutations in four of the six genes determined via sequencing.

Attempt to clone mutations into the boundary reporter S. pombe strain using CRISPR.

Once the presence of the expected point mutations were confirmed in the mutagenized yeast strains, we wanted to reintroduce the mutants into the original boundary reporter strain. This would allow us to determine that the point mutations are sufficient to cause boundary malfunction and not other undiscovered mutations from the previous mutagenesis. We employed multiple cloning techniques to achieve this goal.

First we attempted to use CRISPR/Cas9 to replace the wild type gene in a *epe1Δ IR* boundary reporter with the gene harboring the point mutation because it allowed for modification of the suspected gene without the use of selectable markers. A target specific sgRNA, engineered into the same plasmid as the *cas9* gene, would guide the Cas9 to the target gene in

the *epe1Δ IR* boundary reporter strain. The sgRNA sites were designed close to the point mutations. Cas9 would then cut both DNA strands, triggering homologous recombinant repair mechanisms in the cell. A donor DNA harboring the point mutation, co-transformed with a plasmid expressing the specific sgRNA and Cas9, would act as the repair template, effectively replacing the original gene with the mutant. To do this, the pMZ377 plasmid containing a leucine marker, the *cas9* sequence, and a guide RNA without a targeting sequence, was amplified with primers to introduce the target specific sequence of each suspected gene (Figure 4) then transformed into *E. coli* to build a plasmid that would contain a gRNA to guide CRISPR/Cas9 to each gene we wished to mutate. We sent the resulting plasmids for sequencing to validate that targeting sequences into the gRNA/Cas9. From this, pMZ377 plasmids expressing gRNAs to target the SPNCRNA.189, and *vac7* genes were successful created.

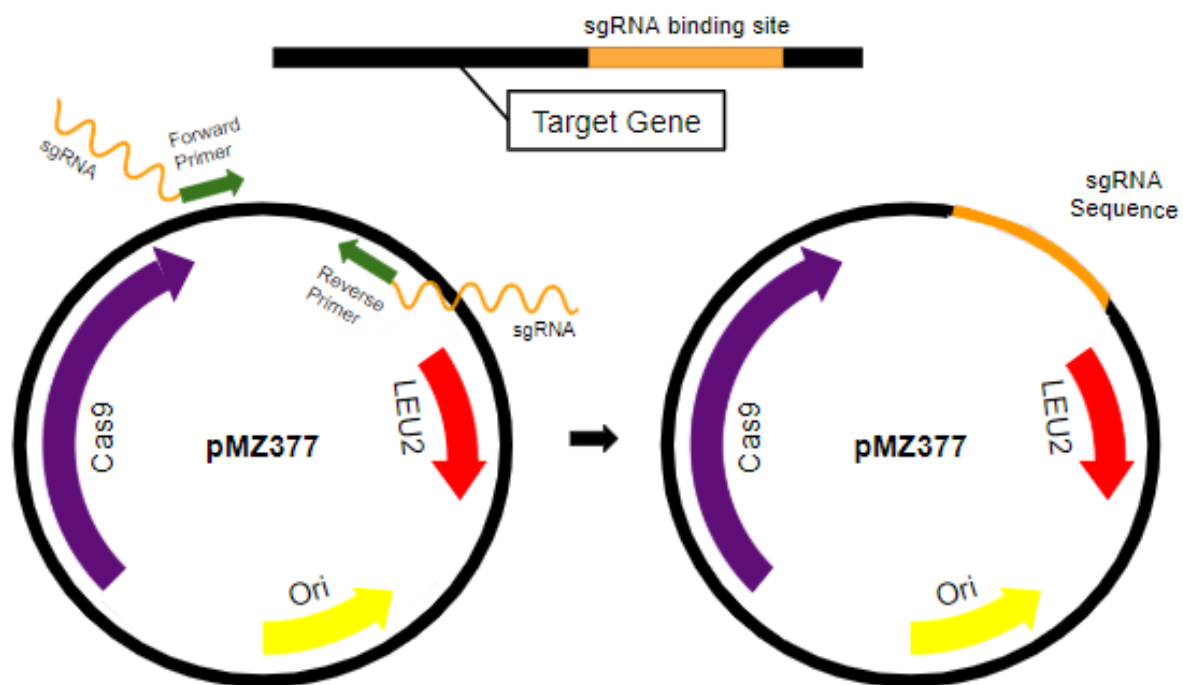


Figure 4: Designing pMZ377 plasmids to introduce sgRNAs to cleave a specific target gene using Cas9. Using CRISPR, sgRNA sites closest to each mutation in the target gene were selected. Primers with these sequences were used to amplify the pMZ377 plasmid expressing the *cas9* gene, a leucine selective marker, and the targeting sgRNA sequence.

With the prepared plasmids, the next step for implementation of this system required the removal of the sgRNA targeting sequence that may be present in the donor DNA. This is required to avoid Cas9-mediated cleavage of the newly inserted DNA due to targeting of the sgRNA to the same site in the donor DNA. To achieve this, we designed a PCR amplification strategy to make the donor DNA. This strategy would generate a donor DNA that contained 4 silent point mutations to prevent binding of the sgRNA but would introduce the point mutation. Three PCRs were designed to achieve this goal for each gene: (1) primers over the sgRNA site and upstream of the point mutation, (2) primers over the sgRNA site and downstream of the point mutation, and (3) the fusion of the two pieces creating the donor DNA product with a scrambled sgRNA site (Figure 5B).

The first two PCRs for all four donor DNA target genes were successfully amplified with the scrambled sgRNA site, as the final PCR products on the gel were the expected size. We had to adjust the annealing temperature in Trial 2 for *sbg1* and to optimize the other reactions with multiple products (Figure 5B). We were unsuccessful in our final attempt to fuse the two PCR fragments by PCR amplification as planned (Figure 5A). There were multiple products in all reactions which required gel purification with the QIAGEN Gel Extraction Kit. The gel purification reduced the amount of DNA so much that the products could not be used as the donor DNA in the CRISPR/Cas9 system. This led us to attempt different method to insert the

mutants into the *S. pombe* boundary reporter strain.

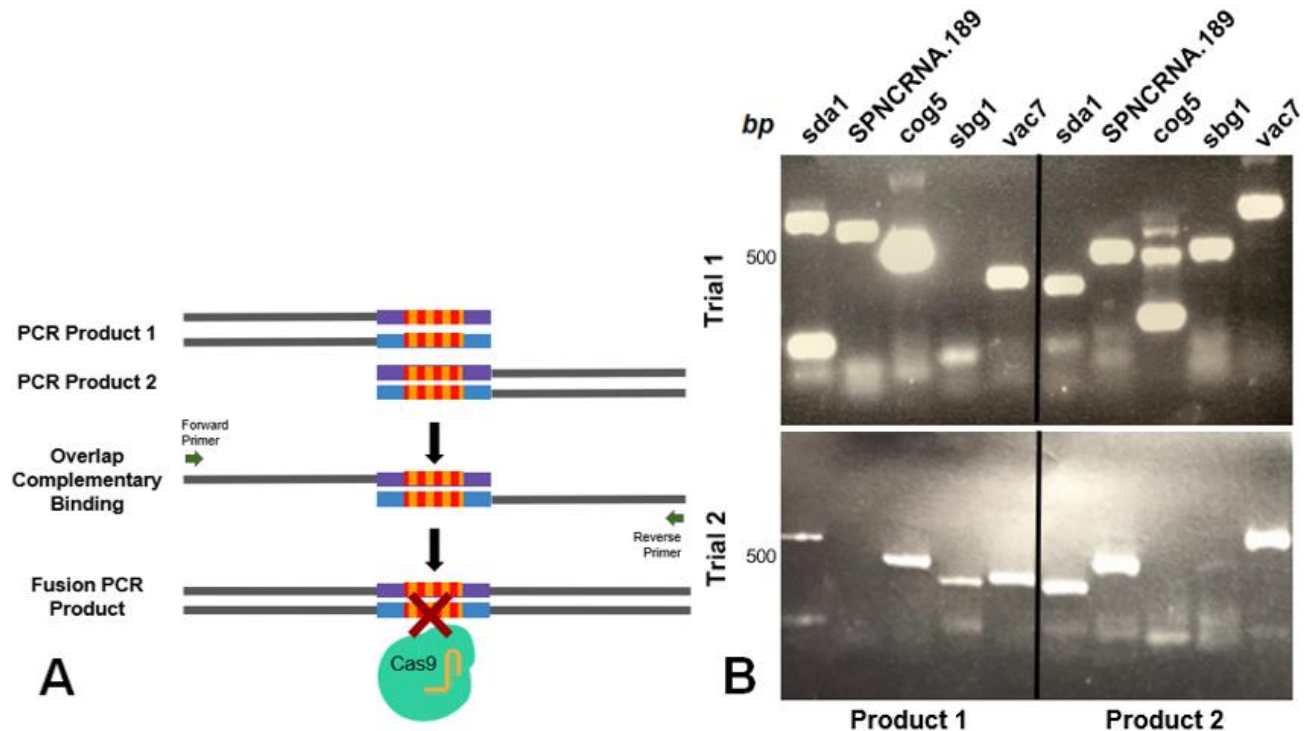


Figure 5: PCR amplification of each target gene with mutated sgRNA primers and a schematic for how each donor DNA was generated. (A) Four silent mutations, red, were introduced into the sgRNA binding sites, blue and purple, and the segments would need to be fused into a whole segment. Cas9 cannot bind and will no longer be able to cut out the introduced mutant, gRNA in yellow. (B) PCR amplification and gel electrophoresis of each gene suspected of inhibiting proper boundary function for fusion and, in Trial 2, the optimization of the PCR for a *sbg1* product.

Attempt to knockout SPNCRNA.189 and vac7 genes in the boundary reporter strain via pAG32.

Instead of using the CRISPR/Cas9 system to reintroduce point mutations identified in *SPNCRNA.189* and *vac7* genes, we wanted to try homologous recombination to delete the two non-essential genes and observe the effect on boundary function. To do this, I would use a DNA cassette, containing the *hphMX* marker flanked with DNA homologous to 5' and 3' ends of the

target gene (Figure 6A). I designed two sets of primers, to amplify the *hphMX* from the pAG32 plasmid with 100 base pair homology to each target gene. Once amplified, the PCR product could be introduced into *S. pombe* strains by transformation, causing the target gene to be deleted and replaced with *HphMX*. The *hphMX* cassette contains the coding region that confers resistance to the drug Hygromycin B, thus allowing for selection for the deletions on YS + HygB agar. I was able to complete the addition of homologous ends to the cassette for the SPNCRNA.189 gene but not *vac7* (Figure 6B). I gel purified the final product before transforming the SPNCRNA.189 deletion cassette, the *IR* boundary reporter with *epe1Δ*, which does not contain the *hphMX* cassette (Table 1), using the *S. pombe* transformation protocol 1. I replica plated the colonies onto HygB but we observed no growth. This result suggested that generating the deletion was unsuccessful by transformation. To remedy this, I decided to focus on improving the transformation efficiency.

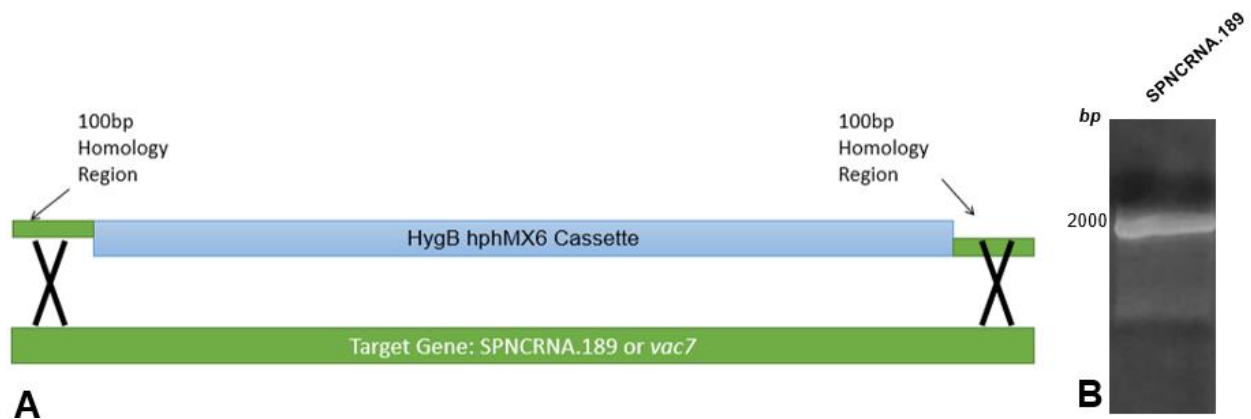


Figure 6: Homologous recombination of the HygB hphMX6 Cassette to delete SPNCRNA.189. (A) A schematic of homologous recombination with HygB after homology regions have been attached to the cassette. (B) Gel electrophoresis of the HygB cassette with SPNCRNA.189 homology regions successfully attached, at 1920bp.

Attempt to clone mutations with SLIC for sda1 and cog5.

The essential genes *sda1* and *cog5*, unlike SPNCRNA.189 and *vac7*, needed to be inserted into a plasmid for cloning. I designed piecewise constructs to include the selectable marker *LEU2* (Figure 7). Using SLIC, sequence ligation and independent cloning, fragments of the target gene with the identified point mutation would be fused to the *LEU2* gene and another copy of the gene's 3' intergenic region (IGR) of the same target gene to allow for homologous recombination in the boundary reporter strain. The full construct would be inserted into the pRS416 plasmid, which contains an *AmpR* marker, for selection and growth in bacteria. The plasmid containing the construct could be purified then cut out by restriction enzymes and transformed into yeast. I PCR amplified the *sda1*-G1160T and *cog5*-G23T genes from their respective strains as well as their 3'IGRs. *LEU2* was amplified from the pMZ377 plasmid. The first forward primer and reverse primer for the IGR had an additional overhang complementary to the pRS416 vector to allow for insertion into pRS416 by SLIC. The amplification of the full gene was not successful, but I was able to amplify four smaller segments of the gene for SLIC ligations. I also amplified the *LEU2* and the 3'IGR effectively, and all segments were added to the SLIC reaction with the *Sma*I digested pRS416 plasmid. Unfortunately, after several rounds of varying incubation periods and enzyme concentrations, the SLIC reaction did not integrate the construct into the plasmid. Despite unsuccessful SLIC reactions, I continued to other methods of creating the full construct outside of the vector, including fusion PCRs. The fusion PCRs are in the process of optimization for adequate product quantity for transformations into the vector.

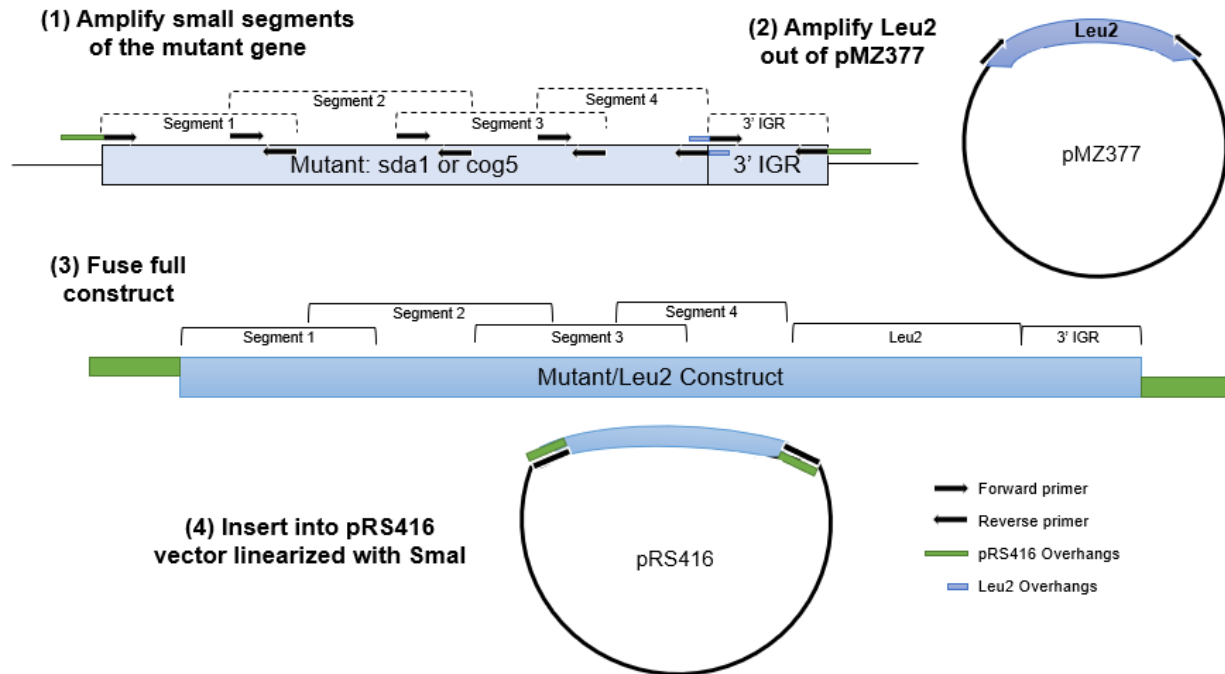


Figure 7: Fusion PCR construct design of the *cog5* and *sda1* mutants and their insertion into the pRS416 vector.

Test and optimize S. pombe transformations.

Once the DNA constructs needed for genetic modification were completed or the processes of obtaining them were fully optimized, we needed to have an optimized transformation procedure to insert them into the reporter for testing. Since our first attempts to transform using the *S. cerevisiae* high efficiency transformations and *S. pombe* transformations had only moderate success, I attempted to improve transformation efficiency with three protocols using a wild type *E. coli* plasmid, B14 that harbored a *LEU2* selectable marker. These three were the *S. pombe* transformation protocol using modified LiOAc, Lithium Acetate Procedure from Nurse Fission Yeast Handbook, and *S. pombe* transformation protocol with nitrogen starved cells (Figure 8A). The *S. pombe* transformation protocol using modified LiOAc produced the most colonies. We then optimized this protocol by testing different OD₆₀₀ levels (*i.e.* concentration of cells in culture) and different volumes of cell culture. We found an

OD₆₀₀=0.5 in 50mL produced the most colonies on *Leu2* selection media and will need to be used for the constructs to be successfully integrated into the reporter strain (Figure 8B).

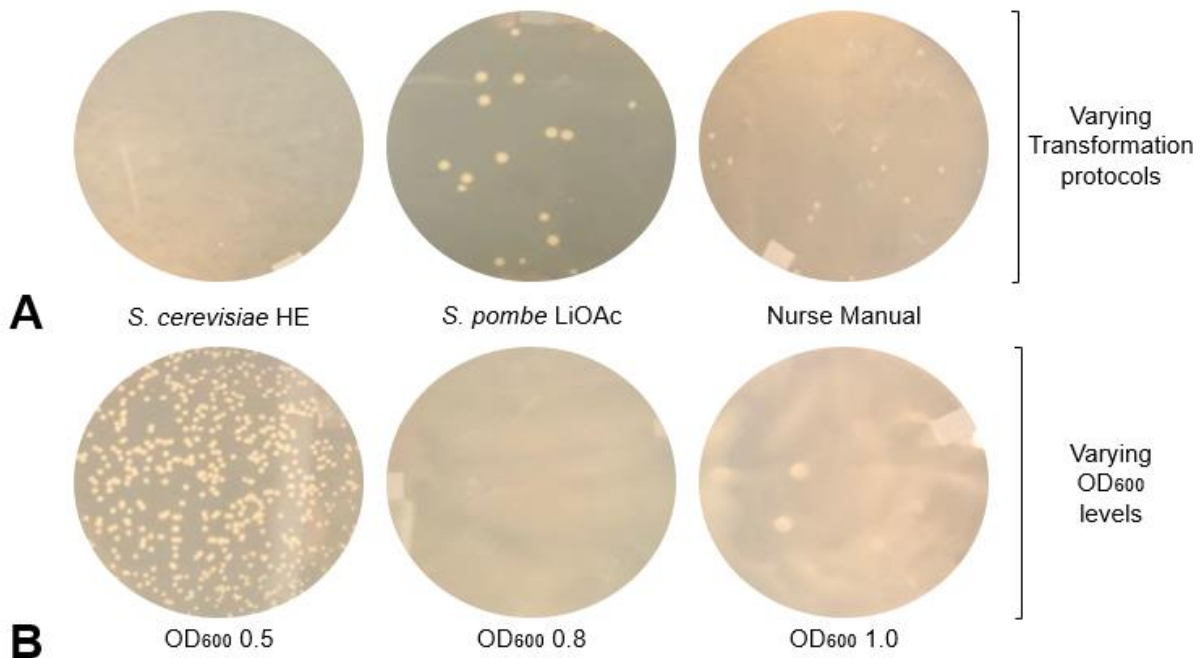


Figure 8: Testing and optimizing transformations of B14 on SC-Leu. (A) Results of the *S. cerevisiae* high efficiency transformation, *S. pombe* transformation protocol using modified LiOAc, and Lithium Acetate Procedure from Nurse Fission Yeast Handbook showed the second to be the most optimal. (B) Tests of different OD₆₀₀ measurements before transformation confirmed that an OD₆₀₀ of 0.5 was the most efficient for the *S. pombe* transformation protocol using modified LiOAc.

Optimization of ChIP.

In order to confirm that the 4 hits I have focused on and that their reintroduced counterparts from the optimized transformations were silencing the reporter by the spread of H3K9me, I performed chromatin immunoprecipitation, ChIP, followed by qPCR to observe H3K9me levels of the *URA4* reporter gene. Our hope is to use ChIP-qPCR once the *sda1-G1160T* and *cog5-G23T* mutants are successfully reintroduced to the reporter strain and

SPNCRNA.189 and *vac7* are deleted. We expect to observe more *URA4* DNA associated with H3K9me chromatin, or earlier amplification curves, from the ChIP-qPCR analysis when heterochromatin spreads over the *URA4* reporter gene in *epe1Δ* IR boundary reporter strains harboring mutants required for boundary function.

To ensure that the ChIP procedure was working, we performed ChIP using two control samples, PM1572, the wild type IR boundary reporter (BR+*epe1Δ*) with full boundary function, and PM1813, the IR reporter strain BR+*epe1Δ*+*B-boxΔ* with a complete loss of boundary function. First, ChIP was done on chromatin prepared by MNase to shear the DNA. The immunoprecipitated DNA purified from this process was analyzed by qPCR using two sets of primers: *URA4* primers that will amplify our reporter gene and *ACT1* primers that will amplify the housekeeping gene *Actin* that should have no methylation, making this a normalization control. Earlier amplification curves indicate more DNA was bound to chromatin marked with H3K9me. However, for this ChIP, qPCR revealed late amplification curves for both primers, suggesting that our ChIP samples didn't contain much DNA. Additionally, the melt peaks presented indicates the number of qPCR products obtained from each amplification. For our experiments we only expect one peak to be present per reaction as this indicates the amplification of a single product. The melt peaks we observe for the *URA4* qPCR shows one peak at 86°C corresponding to the proper amplification of the reporter gene and a secondary melt peak at 76°C. The secondary peak is indicative of a secondary qPCR product (Figure 9). Collectively, these results suggested that our ChIP and our qPCR required more optimization to increase DNA yields and improve our qPCR to generate a single product.

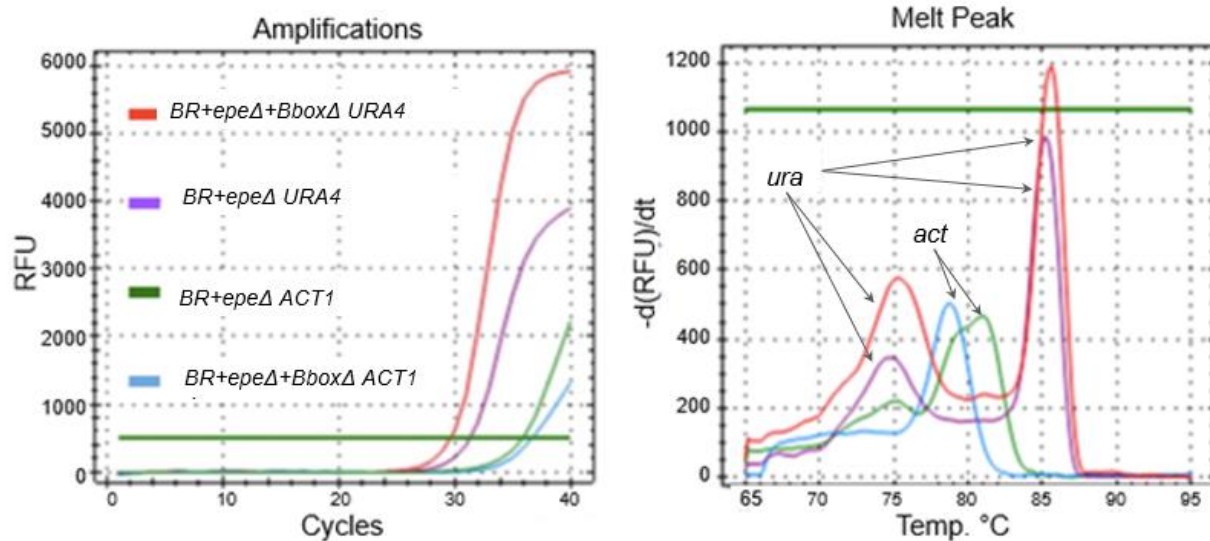


Figure 9: Amplification of boundary reporter strain ChIP samples after optimization using qRT-PCR standard curves with varying -MNase concentration. qRT-PCR of ChIP control samples: boundary reporter (*BR+epe1Δ*) and the double mutant (*BR+epe1Δ+B-boxΔ*) known to have H3K9me across *URA4*. Melt peaks indicate two products when amplified with *URA4* primers for both the *BR+epe1Δ* and *BR+epe1Δ+B-boxΔ* (purple and red), and thus not a completely optimized protocol. A range of 25-120U/μL was tested and 75U/μL was the optimal concentration.

Next, we performed a ChIP experiment where the chromatin was prepared by sonication. To test if sonication can give us more DNA, we used the same strains as in the MNase ChIP procedure, ran ChIP with sonication, then ran qPCR on the immunoprecipitated DNA with the *URA4* and *Actin* primers. The sonication protocol revealed similar amplification curves, but the amplification curves rose earlier suggesting there is more DNA for amplification; this was confirmed by a successful standard curve of the boundary reporter and double mutant (Figure 10A and B). Additionally, a singular melt peaks at 76°C suggests one qPCR product for the *URA4* and *ACT1* primers (Figure 10C and D). As expected in both cases, the amplification with *Actin* as the control was low (Figure 10E). The wild-type *IR* boundary reporter, which would

have low methylation on the *URA4* gene due to active boundary function, showed lower DNA amplification compared to the double mutant lacking boundary function (Figure 10E). This suggests that the double mutant contained more DNA in that was H3K9 methylated and extracted during ChIP, as we would expect with the lack of boundary function and uncontrolled spread. Overall, the qPCR results of the sonication ChIP protocol suggests this assay can be reliably used to quantify H3K9me, and thus boundary function, in our screen hits. We further quantified the data from the sonication and found that the double mutant has greater methylation over the reporter (Figure 11A). The results were not significant (Figure 11B) with this one data set, thus the experiment will be need to be repeated for precision.

Next, we performed ChIP on the screen hits containing the point mutations for *sda1*, SPNCRNA.189, *cog5*, and *vac7* to test if heterochromatin spread over the boundary element is observable. *sda1*, *cog5*, and *vac7* do appear to have more methylation compared to the boundary reporter but not as extensive as the double mutant with complete loss of boundary function. SPNCRNA.189 appears to have less methylation than both controls (Figure 11). Though not statistically significant, these data indicate that three of the mutations identified may exhibit methylation on the *URA4* reporter gene.

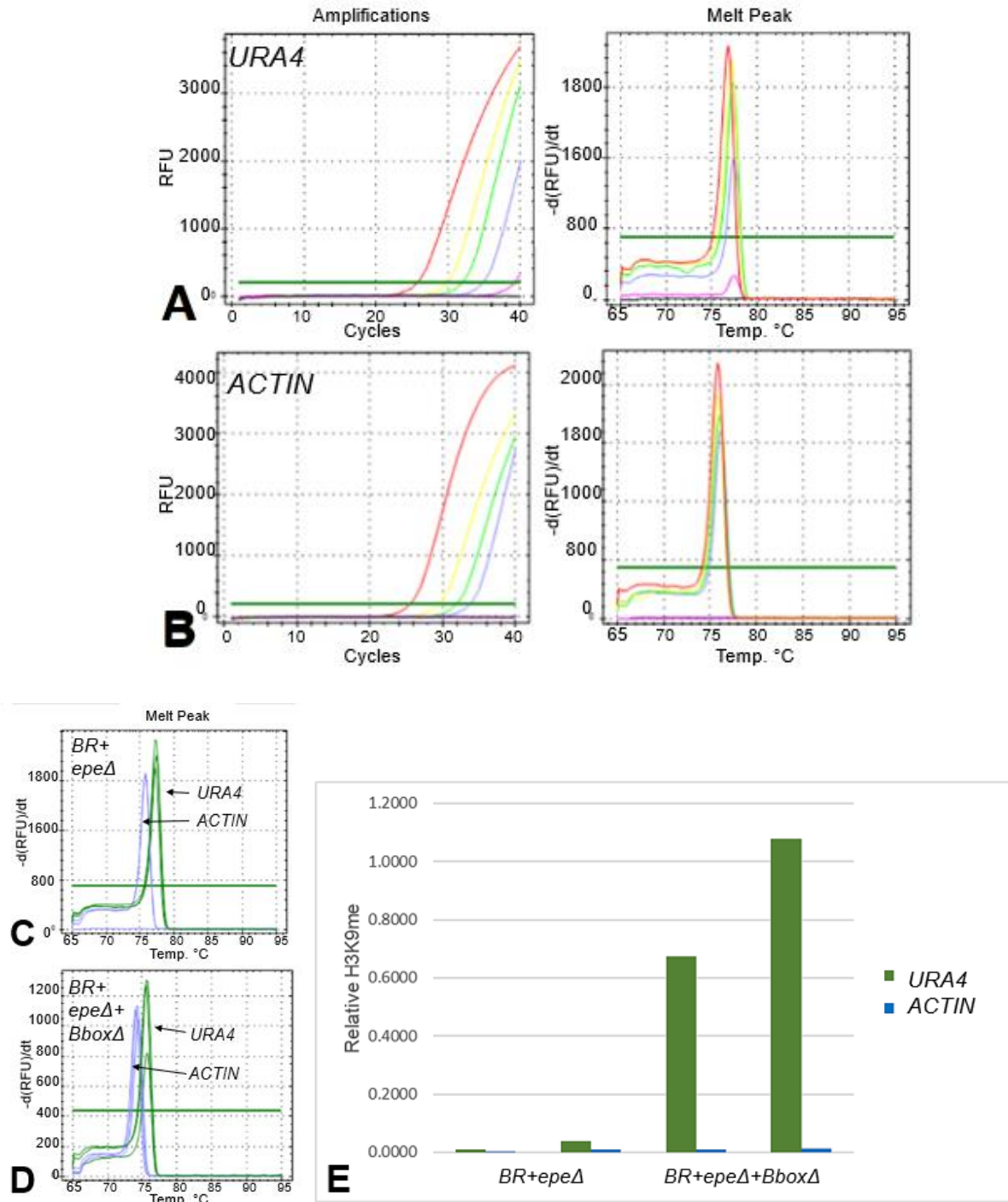


Figure 10: Amplification of boundary reporter CHIP samples after optimization with sonication using qRT-PCR. qRT-PCR of standard curves of the boundary reporter and double mutant, known to have H3K9me across *URA4*, whole cell extracts combined and amplified with primers for (A) *URA4* and (B) *ACT1*. qRT-PCR melt peaks of the (C) wild type boundary

reporter (BR+*epe1*Δ) and (D) double mutant (BR+*epe1*Δ+B-box Δ) immunoprecipitated ChIP samples where green curves indicate a single amplification product of the *URA4* gene and blue curves indicate amplification of *Actin*. (E) Bar graph representing more DNA present in the qRT-PCR of the double mutant (BR+*epe1*Δ+B-box Δ) than the wild type boundary reporter (BR+*epe1*Δ) using the *URA4* primer.

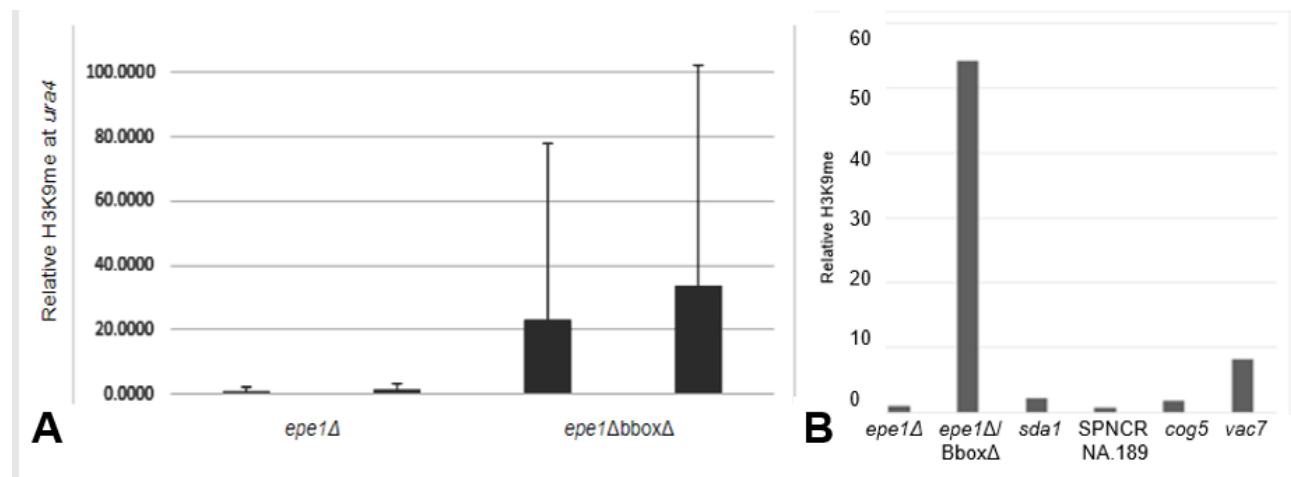


Figure 11. Quantification of the Chromatin Immunoprecipitation of the boundary reporter (*epe1*Δ), double mutant and the mutagenized strains. (A) This data represents the

methylation data collected from ChIP in the boundary reporter (*epe1*Δ) and the double mutant in two different trials. Error bars on the two controls indicate the results were not significant. (B)

This data represents the IP to whole cell extract starting quantity ratio of *URA4* divided by the IP to whole cell extract starting quantity ratio of *ACT1*, normalized to boundary reporter (*epe1*Δ).

epe1/B-boxΔ is known to have H3K9me across *URA4*. H3K9me across *URA4* is unknown in other mutants.

Discussion.

Previous research on H3K9me studied the Epe1 and TFIIC-dependent boundary pathways, both of which function to limit methylation spread beyond set boundaries in the

genome. Uncontrolled spread was shown to be toxic to *Schizosaccharomyces pombe* and possibly a detriment to human genomic stability as well [1,4]. Our main goal throughout this research project was to find specific genes that are important functional components of the TFIIIC pathway of boundary function in *S. pombe*. The previous mutagenesis assay performed by the Garcia Lab in the *CAN1* reporter strains revealed strains that harbored 10 potential mutations that may affect TFIIIC boundary function. These potential mutations arose by selecting for EMS-generated mutants in the boundary reporter strain that grew on + 5-FOA. These strains harboring potential mutants were then sequenced, and were able to narrow down our list of potential mutants that affect boundary function to 4: *sda1*, *cog5*, SPNCRNA.189, and *vac7*. Using ChIP and reintroducing each mutant into the original boundary reporter strains, we attempted to confirm that these mutants were indeed disrupting TFIIIC dependent boundary function and causing spread of H3K9me. We observed the levels of methylation in the original mutant strains from the selection and found three with elevated H3K9 methylation over our reporter gene compared to a strain that harbored a functional boundary element. Secondly, many methods were attempted to clone the mutated genes into the boundary reporter strain to quantify changes in methylation compared to the boundary reporter strain.

Any mutants in the uracil biosynthesis pathway, which interfere with the reporter, or silent mutations were eliminated. After the initial screen on + 5-FOA, we also eliminated mutants of *sbg1* and *kap104* mutants as potential inhibitors in the TFIIIC pathway via Sanger sequencing of PCR amplified genomic DNA because the point mutations were not present. This led us to focus on mutants in *sda1*, SPNCRNA.189, *cog5*, and *vac7*.

Next we focused our attempts to clone the remaining four mutants into the original boundary reporter strains. First, we started by using the CRISPR/Cas9 system. We first amplified gRNA sequences corresponding to the mutants into the pMZ377 plasmid for Cas9. These plasmids and the gRNA integrations for SPNCRNA.189 and *vac7* were successful, seen through sequencing results, suggesting the Cas9 element of the CRISPR mechanism was

ready to be used in these strains. The final step was creating donor DNA fragments with the point mutation and without a sgRNA site that Cas9 would also cut after integrating in the point mutation. Scrambling the sgRNA site via two PCRs in the four original mutagenized strains, *sda1*, SPNCRNA.189, *cog5*, and *vac7*, was successful creating two fragments, though the final fusing of the two fragments was unsuccessful. This ended our attempts to clone the mutants into the boundary reporter with the CRISPR mechanism. If the fusion could be accomplished using a different technique to yield large amounts of a singular product it could still be used, but we continued with other cloning procedures.

Some of these cloning techniques included SLIC and gene deletion by homologous recombination. Neither of these was optimized up to this point in the project, but there were promising results in the homologous recombination procedures. SLIC was overall unsuccessful due to time limitations but *sda1* and *cog5* mutant fragments are currently being ligated into vectors using PCR. The next step would be to optimize these PCRs for ligation into vectors. Deletion of SPNCRNA.189 by homologous recombination seemed to work until the transformation step to introduce the DNA into *S. pombe*. For our initial transformation, we obtained one colony for screening which revealed a negative result. We also attempted to delete the *vac7* gene, but we were unable to amplify homology primers with the hphMX6 cassette. This reaction could be optimized like the SPNCRNA.189 if the primers are redesigned for more efficient annealing in a different location. We, however, chose to troubleshoot the transformation step before restarting optimization of *vac7* gene deletion primers. We improved the transformation by optimizing the protocols to increase the final number of colonies after transformation, and the *S. pombe* transformation using modified LiOAc should be used at an OD₆₀₀ of 0.5.

Once we obtained strains harboring each suspected mutations by cloning, we aimed to observe levels of H3K9me over our reporter gene that monitors boundary function via the CHIP procedure we optimized. We obtained preliminary data for the four mutants suggesting three of

the four strains, harboring mutants in *sda1*, *cog5*, and *vac7*, have more H3K9 methylation spread over our reporter strain. However, the level of H3K9me was not very high, and the procedure will need to be replicated several times because the results were imprecise, leading to insignificant results. However, it is promising that the general phenotype is present in the ChIP assay because it does suggest the phenotypic plating is due to H3K9me spread and not other factors. Overall this data suggests that each of these mutants may affecting boundary function to some degree but not as strongly as removing both Epe1 function and the B-boxes that TFIIIC bind. This result gives us confidence that cloning each of the mutants into the boundary reporter strains will be an efficient way to determine if these mutants affect boundary function.

Wild type functions of each suspected gene and the Results of the Point Mutations.

If any of these suspected genes is confirmed to reduce TFIIIC boundary function, their role in mediating TFIIIC boundary function will need to be examined. Of the four point mutations confirmed, the most interesting is a mutation within the non-coding RNA, SPNCRNA.189. The structure of this ncRNA contains several loops and hairpins that could be altered by a single base pair change; these preliminary predictions were observed using the gene sequence and RNA fold prediction software [14,15]. As other non-coding RNAs have been shown to be important for genome function (i.e. lncRNAs in biogenesis and miRNA used to target unprocessed mRNA for degradation), this non-coding RNA could act as a scaffold and affect binding and molecular interactions that allow boundary function to occur. Recent evidence has shown non-coding RNAs can lead to the condensing of the genome through paraspeckles. Paraspeckles are examples of RNA-protein interactions that increase phase separation. These phases form compartments that help define chromatin domains and distinctly separate certain proteins and RNAs into those domains. This would help separate elements that promote heterochromatin spread from euchromatic regions or facilitate localization of boundary function elements. Although their specific roles in gene regulation require further research, it is possible

that the SPNCRNA.189 point mutation is disrupting proper ncRNA transcription and, thus, interfering with the paraspeckles and localization of elements in the TFIIC pathway [16].

Pending confirmation that SPNCRNA.189 mutation results in loss of boundary function, future studies we hope to focus on may include how SPNCRNA.189 interacts with TFIIC and how the folding of the RNA or formation of paraspeckles may be disrupted by the point mutation.

The other three genes code for proteins, which may easily be truncated by a point mutation, fold differently, or lack activity due to replacement of an amino acid residue. The type of change that occurs via the point mutation will be an important aspect of this project to study in the future because it could provide insight into their function within the pathway. The *sda1*-G1160T mutation in the ORF of the SDA1 family protein involved in ribosome biogenesis and nucleocytoplasmic transport is a missense A227S substitution changing the neutral side chain to polar and uncharged. The *cog5*-G23T mutation in the ORF of a Golgi transport complex subunit, however, is a missense S8I substitution that changes the uncharged and polar group for a neutral one. Finally the *vac7*-A381G is a mutation in the ORF of the PAS complex phosphatidylinositol phosphate kinase activator; it is a missense Q27R substitution that changes the uncharged and polar group for a charge one. Changes like this can drastically change the characteristics of a protein. After these mutations can be confirmed to impact the spread of H3K9me, further investigation will be needed into how each of these changes directly impacts the pathway.

Broader impacts.

Overall, understanding what affect the point mutations from the mutagenesis assay had on the proteins' or RNA's function in the TFIIC pathway will allow us to create a better model of the mechanism as well as understand which steps in the spread of heterochromatin are being disrupted by TFIIC. This detailed information may also highlight other protein and RNA elements in the pathway to investigate next as the mechanism becomes more clearly understood.

Our project, focused on 6 potential mutants that may affect boundary function in the TFIIC pathway. Though our initial screen isolated only 10 potential hits, a larger screen can be employed using our TFIIC boundary reporter strains as we may have only identified a small fraction of what can be found because a smaller scale mutagenesis assay was originally performed. Interestingly genetic screens would also usually yield multiple hits to the same gene, we don't see that other than the mutants of the uracil biosynthesis pathway. This further indicates that we need to do a larger screen. If these mutants truly affected boundary function, we should see multiple hits to the same gene. This research and its future work will aid in mapping out the full TFIIC boundary function in yeast so the fundamental interactions can possibly be generalized to other species, especially humans.

The heterochromatin nucleation and spread is conserved from *S. pombe* to mammals and the H3K9 methylation seen in *S. pombe* are the same for constitutive heterochromatin found in higher eukaryotes [1,2]. The study of TFIIC boundary function is relevant to humans because yeast are a typical model organism for studying the human genome, and little is known about constitutive heterochromatin regulation in humans as well. It was confirmed in previous work that malfunctions in restricting heterochromatin spread is impactful in the silencing of tumor suppressor genes, and research into these processes could be a crucial step in combatting various types of cancer [1]. Once we understand the basics of this mechanism in our model organism, we can begin to efficiently hypothesize and map out which elements in the body help prevent this uncontrolled silencing. Additionally, uncontrolled silencing may also lead to silencing of other critical genes leading to genetic diseases beyond cancer. A more specific example of our research and this mechanism's relevance to humans is the Clr4 enzyme. Clr4, which is critical in the methylation mechanism, has two homologs in mammals, SUV39H1 and SUV39H2; these homologs could allow us to generalize our results and similar studies for observation in mammalian genomes [3]. This is one aspect of the mechanism that has already

given us a starting point for investigating gene regulation in humans, and with this research and future studies in *S. pombe*, more are likely to follow.

Acknowledgements.

This research was made possible by the Figge-Bourquin Summer Research Stipend Award from the Health Professions Committee, the Benezet Start-up Award from the Dean's Office, and the Faculty Research Award provided by Colorado College. I would like to thank Dr. Garcia for providing the supplies, facilities, and mentorship throughout this thesis project. I would also like to thank Alex Barone-Camp as a major contributor to the lab work, presentation of this research figures, and abstract writing during the first summer. Thanks to Peter Lehman for collaborative lab work on the ChIP procedure as well. Finally, I would like to thank the Molecular Biology Department and Carrie Moon for technical support throughout this project.

Tables.

Table 1. *S. pombe* Strain List

Catalog #	Strain PM	Gene Name	Genotype
SP8	PM2101	sda1 (BR + epe1Δ Screen hit #3)	Parental genotype: h-, can1::ura4+-IR-L-4xGAL UAS-ade6+, clr4Δ::hphMX-Gal4DBD-clr4-cdΔ, epe1Δ::kanMX, ade6-M210, leu1-32, ura4-D18, smt0
SP9	PM2102	SPNCRNA.189 (BR + epe1Δ Screen hit #4)	Parental genotype: h-, can1::ura4+-IR-L-4xGAL UAS-ade6+, clr4Δ::hphMX-Gal4DBD-clr4-cdΔ, epe1Δ::kanMX, ade6-M210, leu1-32, ura4-D18, smt0
SP10	PM2104	cog5 (BR + epe1Δ Screen hit #6)	Parental genotype: h-, can1::ura4+-IR-L-4xGAL UAS-ade6+, clr4Δ::hphMX-Gal4DBD-clr4-cdΔ, epe1Δ::kanMX, ade6-M210, leu1-32, ura4-D18, smt0
SP11	PM1572	Boundary Reporter (BR)	h-, can1::ura4+-IR-L-4xGAL UAS-ade6+, clr4Δ::hphMX-Gal4DBD-clr4-cdΔ, ade6-M210, leu1-32, ura4-D18, hphMXsmt0
SP28	PM1813	Double Mutant (BR + BBoxΔ + epe1Δ)	h-, can1::ura4+-IR-L MT1 (-327bp)-4xGAL UAS-ade6+, clr4Δ::hphMX-Gal4DBD-clr4-cdΔ, epe1Δ::kanMX, ade6-M210, leu1-32, ura4-D18, smt0
SP38	PM2099	sbg1 (BR + epe1Δ Screen hit #1)	Parental genotype: h-, can1::ura4+-IR-L-4xGAL UAS-ade6+, clr4Δ::hphMX-Gal4DBD-clr4-cdΔ, epe1Δ::kanMX, ade6-M210, leu1-32, ura4-D18, smt0
SP39	PM2100	kap104 (BR + epe1Δ Screen hit #2)	Parental genotype: h-, can1::ura4+-IR-L-4xGAL UAS-ade6+, clr4Δ::hphMX-Gal4DBD-clr4-cdΔ, epe1Δ::kanMX, ade6-M210, leu1-32, ura4-D18, smt0
SP42	PM2106	vac7 (BR + epe1Δ Screen hit #8)	Parental genotype: h-, can1::ura4+-IR-L-4xGAL UAS-ade6+, clr4Δ::hphMX-Gal4DBD-clr4-cdΔ, epe1Δ::kanMX, ade6-M210, leu1-32, ura4-D18, smt0
SP6	PM2004	IR-R reporter + epe1Δ	h-, IR-R::IR-R-ura4+, epe1Δ::kanMX, ade6-M210, leu1-32, ura4-D18, smt0

*Strains created by Garcia et. al. and the Garcia Lab

Table 2. Primer List

Purpose	Primer Name	Sequence
Gene Amplification	CC78_SPNCRNA.1433_amp_for	5'-TTATACGGCTGAATAGTCAG-3'
	CC79_SPNCRNA.1433_amp_rev	5'-GCATCTTCCTCAAGCCCTTC-3'
	CC83_kap104_amp_for	5'-TCTTGAATTGCTTGAATG-3'
	CC84_kap104_amp_rev	5'-TATTGACAATGCTTCCAAG-3'
(Confrim sgRNA Scramble)	CC88_vac7_amp_for	5'-CTGCTAATCAGGAGGATATG-3'
	CC89_vac7_amp_rev	5'-TTGACCGAGTACACAGCATC-3'
	CC93_SPNCRNA.189_amp_for	5'-GTCCAATCTTACCACAAGAG-3'
	CC94_SPNCRNA.189_amp_rev	5'-ATTCTTCAGGCGCTATACTG-3'
	CC60_sda1_for_1	5'-CAATCTTCCTCATCTACAACATCTG-3'
	CC23_sda1_g>t_rev	5'-CCTTGAGGGTCATGAAGAAGCTG-3'
	CC61_cog5_5utr_for	5'-CGAATAGAAGTGCTAGAATACACTG-3'
	CC21_cog5_c>a_rev	5'-ACTCCCCAAGCCAATACAAAG-3'
Sequencing	CC80_SPNCRNA.1433_seq_for	5'-TTGATCTATTCAAGCGCTGC-3'
	CC85_kap104_seq_for	5'-ACTACCTGCCTTCCCACAC-3'
	CC90_vac7_seq_for	5'-TGTCTGTTGAGACTGAGACG-3'
	CC95_SPNCRNA.189_seq_for	5'-TTGATGGCCATAAGAGCCAC-3'
	CC96_cog5_seq_for	5'-AGGCTGAACGAGTGTTAATC-3'
	CC97_sda1_seq_for	5'-GCAGCAATGGAATCACTATG-3'
gRNA Insert into pMZ377	CC76_SPNCRNA.1433_gRNA_for	5'-ACACGTAGCCGATGTAAGTCTTGTAGAGCTAGAAATAGCAAGTTAAAATAA-3'
	CC77_SPNCRNA.1433_gRNA_rev	5'-TCAGTACATCGGCTACGTGTTCTTCGGTACAGGTTATGTTTTTTGGCAACA-3'
	CC81_kap104_gRNA_for	5'-ATTCCTAGTCTGAGAGTTTTGTTTTAGAGCTAGAAATAGCAAGTTAAAATAA-3'
	CC82_kap104_gRNA_rev	5'-AAAACCTCTCAGACTAGGAATTTCTTCGGTACAGGTTATGTTTTTTGGCAACA-3'
	CC86_vac7_gRNA_for	5'-AGTGGCCTCTGCCGTTGATCGTTTTAGAGCTAGAAATAGCAAGTTAAAATAA-3'
	CC87_vac7_gRNA_rev	5'-GATCAACGGCAGAGGCCACTTTCTTCGGTACAGGTTATGTTTTTTGGCAACA-3'
	CC91_SPNCRNA.189_gRNA_for	5'-CTTAAGTAACAAGCACATGGGTTTTAGAGCTAGAAATAGCAAGTTAAAATAA-3'
	CC92_SPNCRNA.189_gRNA_rev	5'-CCATGTGCTTGTACTTAAGTTCTTCGGTACAGGTTATGTTTTTTGGCAACA-3'

sgRNA Site Scramble	CC105_SPNCRNA189_sgRNA_mt_For	5'-TGTCTAAATTTTTCTTAAGTCACCAGTACCTGGTGGCACTTGGAAAGTAAC-3'
	CC106_SPNCRNA189_sgRNA_mt_Rev	5'-AGTGCCACCAGGACTGCTGACTTAAGAAAAATTTAGACAGTTAC-3'
	CC103_sbg1_sgRNA_mt_For	5'-AAATATGCCTTCCGTCCACCGACTACGTGTGCCCATTC AAG-3'
	CC104_sbg1_sgRNA_mt_Rev	5'-TTGAATGGGCACACGTAGTCGGTGGACGGAAGGCATATTTACTAAGTATTC-3'
	CC107_vac7_sgRNA_mt_For	5'-TTGCAGCAAGAGTGGCCTCCGCAGTCGACCGGGATCCAACGATGAAG-3'
	CC108_vac7_sgRNA_mt_Rev	5'-TTTGATCCCGTTCGACTGCGGAGGCCACTCTTGCTGCAAAC-3'
	CC109_sda1_sgRNA_mt_For	5'-AAATCTTCCGCACTATCCTCCAATCCTAAAGTTATGCTTGCAGGGATTAC-3'
	CC110_sda1_sgRNA_mt_Rev	5'-CAAGCATAACTTTAGGATTGGAGGATAGTGC GGAAGATTTTCATG-3'
	CC111_cog5_sgRNA_mt_For	5'-ATATCGAGGGAAAACTGGAGCAGTTAATTTTGGTTTATGAAAAGAAATTCG-3'
	CC112_cog5_sgRNA_mt_Rev	5'-CATAAACCAAATAAAGTCTCCAGTTTTCCCTCGATATCTTG-3'

hphMX Deletion Set1	CC114_SPNCRNA189-KO-MX-F1	5'-TCTCGCTAACCTGACTACACTTCCTTAATAAATAGGAGCGCGGATCCCCGGGTTAATTAA-3'
	CC115_SPNCRNA189-KO-MX-R1	5'-TCAGGCGCTATACTGTGAATGCAATGTTTCTACGAGGATCTGATATCATCGATGAATTCG-3'
	CC135_vac7_F1_MX_KO	5'-GAGGACACAATTTGTCTATTTCAATCATTATATTAACATGCATTTTAGTACGGATCCCCGGGTTAATTAA-3'
	CC136_Vac7_R1a_MX_KO	5'-CAAGGCCTGACTTCATAATCAAAGAGCCGTATAAGTTGTATCTCACTTCGGATCTGATATCATCGATGAATTCG-3'
hphMX Deletion Set2	CC116_SPNCRNA189-KO-MX-F2	5'-TAAAAAAATTTATTAAGAAAAATTAAGAAAAATAAAAAAACAGAAAAATGTACTTTTTCTCGCTAACCTGACTACAC-3'
	CC117_SPNCRNA189-KO-MX-R2	5'-ACCTAAAATATGTACAACATAGATTCCAGTAATATATATATTGCAAAATGACTGAACTCAATTCCTCAGGCGCTATACTGTGAATG-3'
	CC137_Vac7_MX_KO_F2	5'-GAAAAAAATAGTTTGCCCAATGGTATGCATCTAGCAGCTGCTAGCTTTTGAGGACACAATTTGTCTATTTTC-3'
	CC138_Vac7_MX_KO_R2	5'-CATTAACATAATTCAAAAGGGCATAATAACAAAAGGTTAGCAAACGCTTTACAAGGCCTGACTTCATAATC-3'

Full Fusion	CC153_cog5_F plasmid/fusion	5'-CGATAAGCTTGATATCGAATTCCTGCAGCCCGCGCCGCACTGTAAGTGCCTGACGAATG-3'
(Insert Check)	<i>CC154_cog5_R1 Fusion</i>	5'-TACAATTGCCTCATGAAGGG-3'
	CC155_cog5_F2 fusion	5'-GAATTCGTTTCGCTGGTAGTC-3'
	CC156_cog5_R2 fusion	5'-GTAGGAGTCTTCGTGTAGTG-3'
	CC157_cog5_F3 fusion	5'-AGTTCTCGTATACAGAAGGC-3'
	CC158_cog5_R3 fusion	5'-GTAGCCAATCGTCGATCTTG-3'
(Insert Check)	<i>CC159_cog5_F4 fusion</i>	5'-GACCATCAAGCAATGCTTCC-3'
	CC134_cog5_F_IGR	5'-TGTCAGAAACGGCCCTTAACGACGTAGTCGACTCCTGATACTACTTAATCTCG-3'
	CC132_cog5_R_Plasmid_Insert	5'-GGCGGCCGCTCTAGAAGTGGATCCCCCTATTTTCGGCCATTCCAATTC-3'
	CC160_sda1_F plasmid/fusion	5'-CGATAAGCTTGATATCGAATTCCTGCAGCCCGCGCCGCACTAGGCAAAAGAGCAGGTAC-3'
(Insert Check)	<i>CC161_sda1_R1 Fusion</i>	5'-GAATGGTGAGAGATACCTGTTG-3'
	CC162_sda1_F2 fusion	5'-AATCCTACTCGTGGTGTTCG-3'
	CC163_sda1_R2 fusion	5'-ACTGAGTAACGTCTCTCTGG-3'
	CC164_sda1_F3 fusion	5'-GGTTCTCACAAGTACAGTCC-3'
	CC165_sda1_R3 fusion	5'-TACTCAGTCTGCGATAGTGG-3'
(Insert Check)	<i>CC166_sda1_F4 fusion</i>	5'-TTGTCCGTGCAAGTCCTTC-3'
	CC128_sda1_IGR_F_amp_w/Leu2OH	5'-CTCTGTAGAAACGGCCCTTAACGACGTAGTCGAACATGATTGAGGGATAACCTATGG-3'
	CC126_sda1_R_Plasmid_Insert	5'-CCGCTCTAGAAGTGGATCCCCGAGACCTCTGCTCTTAGCTTATAC-3'
	CC129_LEU2_For	5'-CTTGACCCGAGTAACTGT-3'
	CC130_LEU2_Rev	5'-TCGACTACGTGTTAAGGC-3'
Insert Check	M13F	5'-GTAAAACGACGGCCAGT-3'
	M13R	5'-CAGGAAACAGCTATGAC-3'
qPCR	P581 ura4+ F	5'-CAGCAATATCGTACTCCTGAA-3'
	P582 ura4+ R	5'-ATGCTGAGAAAGTCTTTGCTG-3'
	P86 act1+ F	5'-CAACCCTCAGCTTTGGGCTTG-3'
	P87 act1+ R	5'-TCCTTTGCATACGATCGGCAATAC-3'

***Primers used twice are in italics with second label*

Table 3. Restriction Enzyme Digests

Reaction Procedure	Enzymes Utilized
pRS416 linearization	SmaI
pRS416/sda1 construct test	XbaI & PstI

Table 4. Bacterial Colony PCR of *sda1*

	Primers	Product Size
Insert Check	M13F & CC161	1002bp
	M13R & CC166	459bp

Literature Cited.

1. Bannister, Andrew J, and Tony Kouzarides. "Regulation of Chromatin by Histone Modifications." *Cell Research*, vol. 21, no. 3, 2011, pp. 381–395., doi:10.1038/cr.2011.22.

2. Isaac, Sara, et al. "Interaction of Epe1 With the Heterochromatin Assembly Pathway in *Schizosaccharomyces Pombe*." *Genetics*, vol. 175, no. 4, 2007, pp. 1549–1560., doi:10.1534/genetics.106.068684.
3. Wang, Jiyong, et al. "Chromosome Boundary Elements and Regulation of Heterochromatin Spreading." *Cellular and Molecular Life Sciences*, vol. 71, no. 24, July 2014, pp. 4841–4852., doi:10.1007/s00018-014-1725-x.
4. Garcia, Jennifer F., et al. "Intrinsic Toxicity of Unchecked Heterochromatin Spread Is Suppressed by Redundant Chromatin Boundary Functions in *Schizosaccharomyces Pombe*." *G3&Amp;#58; Genes [Genomes] Genetics*, vol. 5, no. 7, Aug. 2015, pp. 1453–1461., doi:10.1534/g3.115.018663.
5. Zhang, Ke, et al. "Roles of the Clr4 Methyltransferase Complex in Nucleation, Spreading and Maintenance of Heterochromatin." *Nature Structural & Molecular Biology*, vol. 15, no. 4, 2008, pp. 381–388., doi:10.1038/nsmb.1406.
6. Braun, Sigurd, et al. "The Cul4-Ddb1Cdt2 Ubiquitin Ligase Inhibits Invasion of a Boundary-Associated Anti-silencing Factor into Heterochromatin." *Cell*, vol. 144, no. 1, 2011, pp. 41–54., doi:10.1016/j.cell.2010.11.051.
7. Bao, Kehan, et al. "Anti-Silencing Factor Epe1 Associates with SAGA to Regulate Transcription within Heterochromatin." *Genes & Development*, vol. 33, no. 1-2, 2018, pp. 116–126., doi:10.1101/gad.318030.118.
8. Noma, Ken-Ichi, et al. "A Role for TFIIIC Transcription Factor Complex in Genome Organization." *Cell*, vol. 125, no. 5, 2006, pp. 859–872., doi:10.1016/j.cell.2006.04.028.
9. Valenzuela, Lourdes, et al. "Transcription Independent Insulation at TFIIIC-Dependent Insulators." *Genetics*, vol. 183, no. 1, 2009, pp. 131–148., doi:10.1534/genetics.109.106203.
10. Wang, Xiaoyi, and Danesh Moazed. "DNA Sequence-Dependent Epigenetic Inheritance of Gene Silencing and Histone H3K9 Methylation." *Science*, vol. 356, no. 6333, 2017, pp. 88–91., doi:10.1126/science.aaj2114.
11. Biolabs, New England. "High Efficiency Transformation Protocol (C2987H/C2987I)." *NEB*, <https://www.neb.com/protocols/0001/01/01/high-efficiency-transformation-protocol-c2987>.
12. Li, Mamie Z, and Stephen J Elledge. "Harnessing Homologous Recombination in Vitro to Generate Recombinant DNA via SLIC." *Nature Methods*, vol. 4, no. 3, Nov. 2007, pp. 251–256., doi:10.1038/nmeth1010.
13. Gonzales, Miguel F, et al. "Rapid Protocol for Preparation of Electrocompetent *Escherichia Coli* and *Vibrio Cholerae*." *Journal of Visualized Experiments: JoVE*, MyJove Corporation, 8 Oct. 2013, <https://www.ncbi.nlm.nih.gov/pmc/articles/PMC3939052/>.
14. "PomBase, the *S. Pombe* Genome Database." Pombase, www.pombase.org/.
15. RNAfold Web Server, rna.tbi.univie.ac.at/cgi-bin/RNAWebSuite/RNAfold.cgi.
16. Fox, Archa H., et al. "Paraspeckles: Where Long Noncoding RNA Meets Phase Separation." *Trends in Biochemical Sciences*, vol. 43, no. 2, 2018, pp. 124–135., doi:10.1016/j.tibs.2017.12.001.